Simulating the Charge-Resonance Check in Nitrogen-Vacancy Centers using Python

Uroš Ognjanović - 4712846

Bachelor's Thesis
BSc Applied Mathematics and Applied Physics
Faculty EEMCS and AS
Delft University of Technology

July 2020
Supervisors: Ir. A.J. Stolk,
Prof.dr. R. Hanson and
Dr. J.L.A. Dubbeldam

Abstract

In this report we present a model to simulate the performance and robustness of the Charge-Resonance Check (CR-Check) in the Nitrogen-Vacancy (NV) center. The CR-Check is a routine which verifies that the charge state of the NV center is NV^- and that the lasers, addressing the NV center, are on resonance with the optical lines. This is done by shining a red ($\lambda = 637$ nm) laser on the NV center and measuring the amount of fluorescence photons, since they are dependent on the resonance frequency being near the frequency of the laser. If these counts do not pass the threshold for success, then either a new measurement of the photons is done or the system is repumped with a green ($\lambda = 532$ nm) high intensity laser if they are below the repump threshold. In the last situation the charge environment is reset and thus a new resonance frequency is obtained. First a model was built up for the CR-Check, containing all the important physical parameters. The most important parameters are the duration of the red laser (dt) and the spectral diffusion of the NV center (sigma), which is an intrinsic property of the NV center.

The model was implemented in Python, where also Numba, a high-performance Python compiler was used. An algorithm for finding the optimal values is included, so that different implementations can be compared. Then parameter sweeps were performed to get insight on the effects of the parameters.

The values of the memory parameter and of the threshold for the maximal amount of photon measurements before doing a repump were determined experimentally.

The distribution of frequency spectrum was investigated, it follows the shape of the Generalized Normal distribution with a disturbance due to the memory parameter.

We observed that the mean time till success goes up linearly with the sigma after it is higher than 80 MHz for dt. This effect can be explained by taking into account the Normal distribution which was used to determine the resonance frequency.

It became clear that the N_thr_repump and N_thr_success often come as pairs, which have been shown to be linearly dependent on the rate. Also it has been observed that after a certain sigma amount the N_thr_repump and N_thr_success do not change anymore.

We noticed that for fixed sigma there is a optimal value of dt. This optimal value of dt is dependent on sigma.

Average number of photon counts was nearly independent of sigma and only linearly dependent on dt. This is a sign that the CR-Check can always bring the NV center sufficiently on resonance.

It has been observed that when the NV center's spectral diffusion is below 40 MHz, it is significantly faster to use the CR-strategy with dt = 25 µs compared to the standard dt of 50 µs.

Lastly new implementations, where p-values are used rather than the measured counts, were shown to be capable of performing a CR-Check procedure. These implementations have used either the cumulative density function (cdf) of the Poisson distribution or the t-test or the Wilcoxon signed-rank test. The test using the cdf performed very similar to the current implementation. The other two test were slower with regards to the mean time till success, as they seem to require a lower spectral diffusion than was mandated.

Contents

1 Introduction

In the future Quantum Networks could provide a fundamentally secure form of communication, In addition to this they could also link up different quantum computers. The Nitrogen-Vacancy (NV) center is a defect in the crystal lattice in a diamond, where two adjacent carbon atoms are replaced by a nitrogen atom and an empty lattice site. These NV centers can be employed as a solid-state spin-qubits and as such they can be the nodes of a Quantum Network. The NV centers have great potential to be used for quantum technologies due to their optical interface, an easily addressable ground-state spin that is paired with long coherence times and in particular the ability to address individual nuclear spins in the vicinity as a quantum resource [1].

Before any entanglement process can be started the Charge-Resonance Check (CR-Check) must be passed. The CR-Check is a routine which verifies that the charge state of the NV center is NV^- and that the lasers, addressing the NV center, are on resonance with the optical lines. However optimizing this procedure is complex and experimentally not fully understood, whilst the time spent on it is comparable to the time spent to make entanglement. Therefore it would be useful if this process could be accelerated.

The aim of this project is to make a model to simulate the performance and robustness of the CR-Check. Furthermore improvements to the current implementation and alternative protocols will be investigated.

A model has to be built up for the CR-Check, containing all the important physical parameters. First the building blocks in each iteration of the CR-Check are defined. Next the CR-Check routine is defined in a simplified form, which is easier to understand and can serve as a sanity check for the extended version. Thereafter an implementation of the current protocol, which is currently in use in the laboratory, will be made. Also an algorithm for finding the optimal values of the threshold parameters in the CR-Check will be made.

To be able to conclude anything from the observed data many iterations have to be done, such that one might expect that the Law of Large Numbers starts to apply. This requires that the code is as efficient as possible with regards to the computation time. It will be implemented in Python in combination with Numba, a high-performance Python compiler.

This fast code permits sweeps over the parameters space to retrieve some insight of the effects of the parameters. With this knowledge a proposal for amendments of the current procedure will be made. Moreover the alternative protocols will also be tested.

To start, the theoretical background of the mathematics involved in the simulation and the physics of the NV center will be discussed in chapter 2. The algorithm is discussed in chapter 3, as well as the validity of the model. In chapter 4 the results of the simulations CR-Check are presented. Finally the conclusions are presented in chapter 5.

This research is a part of the Bachelor's Thesis for the Double Degree Bachelor's programme Applied Mathematics and Applied Physics at Delft University of Technology.

2 Theory

In the first part of this chapter we will discuss the mathematics involved in the modelling. The Poisson distribution is treated extensively, since it is very important in the model. Also the generalized normal will be briefly discussed. The second part of this chapter treats the most important properties of the NV center, which will be of use to develop the simulation of the Charge-Resonance Check.

For the interested reader both the Weak Law of Large Numbers and the Strong Law of Large Numbers are proven in Appendix A. These are shown to formally prove that the averaging over many iterations in a simulation will give sensible information about the stochastic process, that we are observing.

2.1 Poisson distribution

The Poisson distribution is a discrete probability distribution. It is often used to express the probability that a given amount of events happen in fixed amount of time, when they occur with a constant mean rate and the next measurement is independent of the previous instance. For example radioactive decay is modelled using the Poisson distribution.

The probability mass function (pmf) for the Poisson distribution is given by [3]:

$$\mathbb{P}(X = k) = \frac{\lambda^k}{k!} e^{-\lambda}.$$

We can check that this is a good definition of a pmf, since:

$$\sum_{k=0}^{\infty} \mathbb{P}(X = k) = \sum_{k=0}^{\infty} \frac{\lambda^k}{k!} e^{-\lambda} = e^{-\lambda} \sum_{k=0}^{\infty} \frac{\lambda^k}{k!} = e^{-\lambda} e^{\lambda} = 1,$$

where we have used the definition of the exponent. Now we can use this result to calculate higher order moments of the Poisson distribution.

The expectation of the first moment, the mean, is given by:

$$\mathbb{E}(X) = \sum_{k=0}^{\infty} k\mathbb{P}(X = k) = \sum_{k=0}^{\infty} k \frac{\lambda^k}{k!} e^{-\lambda} = \sum_{k=1}^{\infty} \frac{\lambda^{(k-1)+1}}{k-1!} e^{-\lambda} = \lambda \sum_{n=0}^{\infty} \frac{\lambda^n}{n!} e^{-\lambda} = \lambda.$$

For the calculation of the variance we will use a smart trick, similarly as for the first moment:

$$\mathbb{E}(X(X-1)) = \sum_{k=0}^{\infty} k(k-1)\mathbb{P}(X = k) = \sum_{k=0}^{\infty} k(k-1) \frac{\lambda^k}{k!} e^{-\lambda} = \sum_{k=2}^{\infty} \frac{\lambda^{(k-2)+2}}{k-2!} e^{-\lambda} = \lambda^2 \sum_{n=0}^{\infty} \frac{\lambda^n}{n!} e^{-\lambda} = \lambda^2.$$

So now we easily compute the variance and thus we get:

$$Var(X) = \mathbb{E}(X^2) - (\mathbb{E}(X))^2 = \mathbb{E}(X(X-1)) + \mathbb{E}(X) - (\mathbb{E}(X))^2 = \lambda^2 + \lambda - \lambda^2 = \lambda.$$

So we have computed that both the mean and the variance are both λ for the Poisson distribution.

In the simulations it will be of importance to estimate λ the best we can given a number of observations. For this purpose we shall find the Method of Moments Estimator (MME) and the Maximum Likelihood Estimator (MLE) and of use. The Method of Moments Estimator is easily calculated:

$$\hat{\lambda}_{MME} = \bar{X} = \frac{1}{n} \sum_{j=1}^{n} x_j.$$

The Maximum Likelihood Estimator maximizes the likelihood function, which in our case assigns the probability to the observed values as a function of the parameter λ. This is then optimized for the parameter λ. For the Poisson distribution it is computed by [5]:

$$L(\lambda; x_1, \ldots, x_n) = \prod_{j=1}^{n} \exp(-\lambda) \frac{1}{x_j!} \lambda^{x_j}.$$

By taking the natural logarithm we obtain for the log-likelihood:

$$l(\lambda; x_1, \ldots, x_n) = \ln\left(\prod_{j=1}^{n} \exp(-\lambda) \frac{1}{x_j!} \lambda^{x_j}\right) = \sum_{j=1}^{n} \ln\left(\exp(-\lambda) \frac{1}{x_j!} \lambda^{x_j}\right) =$$

$$\sum_{j=1}^{n} \left(-\lambda - \ln(x_j!) + x_j \ln(\lambda)\right) = -n\lambda - \sum_{j=1}^{n} \ln(x_j!) + \ln(\lambda) \sum_{j=1}^{n} x_j.$$

Now we want to find the maximum of the log-likelihood for λ, thus we take the first derivative with respect to λ [2]:

$$\frac{d}{d\lambda} l(\lambda; x_1, \ldots, x_n) = \frac{d}{d\lambda}\left(-n\lambda - \sum_{j=1}^{n} \ln(x_j!) + \ln(\lambda) \sum_{j=1}^{n} x_j\right) = -n + \frac{1}{\lambda} \sum_{j=1}^{n} x_j.$$

So equating this expression to 0 and rewriting it gives:

$$\hat{\lambda}_{MLE} = \frac{1}{n} \sum_{j=1}^{n} x_j.$$

So both MME and MLE for λ are the average of the observations.

And we have $\frac{d^2}{d\lambda^2} l(\lambda; x_1, \ldots, x_n) = -\frac{1}{\lambda^2} \sum_{j=1}^{n} x_j \leq 0$, since $x_j \geq 0$. Thus it is indeed a maximum.

Another property of the Poisson distribution is that for large values of λ, it may be approximated by the Normal distribution with mean λ and variance λ. A proof of this statement can be found in Appendix B. In practice the approximation is already acceptable for $\lambda \approx 20$.

Independent Poisson distribution

Since we will mostly deal with the Poisson distribution, it is important to remember that if we add two independent random variables, which are Poisson distributed, we get that their sum is Poisson distributed with the parameter λ equal sum of the individual parameters.

Theorem 2.1.1. *Let $X \sim Po(\lambda_1)$ and $Y \sim Po(\lambda_2)$ and define $Z = X + Y$, then $Z \sim Po(\lambda)$ with $\lambda = \lambda_1 + \lambda_2$.*

Proof. Let $X \sim Po(\lambda_1)$ and $Y \sim Po(\lambda_2)$ and define $Z = X + Y$ and $\lambda = \lambda_1 + \lambda_2$, then let $m \in \mathbb{N}$

$$\mathbb{P}(Z = m) = \mathbb{P}(X + Y = m) = \sum_{n=0}^{m} \mathbb{P}(X + Y = m | X = n) \mathbb{P}(X = n) =$$

$$\sum_{n=0}^{m} \mathbb{P}(Y = m - n | X = n) \mathbb{P}(X = n) = \sum_{n=0}^{m} \mathbb{P}(Y = m - n) \mathbb{P}(X = n) = \sum_{n=0}^{m} \frac{\lambda_2^{m-n}}{(m-n)!} e^{-\lambda_2} \frac{\lambda_1^n}{n!} e^{-\lambda_1} =$$

$$e^{-\lambda_1} e^{-\lambda_2} \sum_{n=0}^{m} \frac{\lambda_2^{m-n}}{(m-n)!} \frac{\lambda_1^n}{n!} = \frac{e^{-(\lambda_1+\lambda_2)}}{m!} \sum_{n=0}^{m} \frac{m!}{n!(m-n)!} \lambda_2^{m-n} \lambda_1^n = \frac{e^{-\lambda}}{m!} \sum_{n=0}^{m} \binom{m}{n} \lambda_1^n \lambda_2^{m-n} =$$

$$\frac{e^{-\lambda}}{m!} (\lambda_1 + \lambda_2)^m = \frac{\lambda^m}{m!} e^{-\lambda}.$$

This is the probability of a Poisson distribution with parameter $\lambda = \lambda_1 + \lambda_2$. So $Z \sim Po(\lambda)$ with $\lambda = \lambda_1 + \lambda_2$. □

This is proof for adding two Poisson distributions, we may conclude from the above that it holds in general for $n \in \mathbb{N}$ since we can keep on adding additional Poisson random variables and applying the above theorem each time on a Poisson random variable and the sum of Poisson random variables.

2.2 Generalized Normal distribution

The Generalized Normal distribution (or Generalized Gaussian distribution) is obtained naturally by replacing the second power in the probability density function of a Normal distribution for a parameter $\beta > 0$, which can have any order [4]. Of course the normalization factor needs to be modified as well. This gives for the probability density function [4]:

$$f(x) = \frac{\beta}{2\alpha\Gamma(1/\beta)} e^{-\left(\frac{|x-\mu|}{\alpha}\right)^{\beta}},$$

where $\Gamma(t) = \int_0^{\infty} \mathrm{e}^{-u} u^{t-1} \mathrm{d}u$ is the well-known Gamma function, $\mu \in \mathbb{R}$ is the location of the mean, $\alpha > 0$ is the scale parameter and $\beta > 0$ the shape parameter. It can be easily seen that for $\beta = 2$ the Normal distribution is again obtained. The scale parameter has the similar effects as the standard deviation in the Normal distribution. The shape parameter flattens the top and makes the distribution sharper, this is illustrated in the following figure.

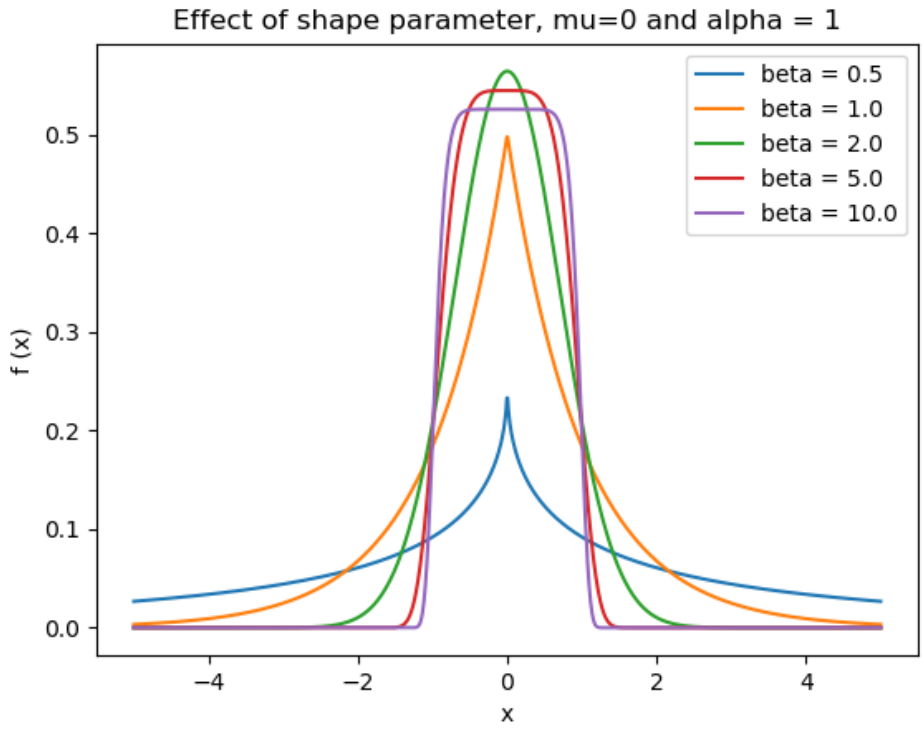

Figure 1: Shows the effect of the shape parameter on the distribution for $\mu = 0$ and $\alpha = 1$.

From Fig.1 can be seen that for equal values of α, different kinds of spread exist. Therefore just α is not a good measure of spread. The first two moments of the Generalized Normal distribution are [4]:

$$\mathbb{E}(X) = \mu$$
$$Var\,(X) = \frac{\alpha^2\Gamma(3/\beta)}{\Gamma(1/\beta)}.$$

Therefore the variance seems to be a reasonable measure of the spread of the distribution, as it takes both the α and β parameter into account.

2.3 Statistical test

The p-value is used to quantify mathematically how likely a value is to occur under a null hypothesis, so for low values p the null hypothesis is rejected for the alternative hypothesis. To get this p-value, first a statistical test has to be defined. Multiple statistical tests will be defined in the following section.

Direct test

Let the random variable X be Poisson distributed, where parameters λ is unknown. We want to test the null hypothesis $H_0 : \lambda \leq \lambda_0$ against $H_1 : \lambda > \lambda_0$, where λ_0 is a fixed. We take X as the test statistic and t the observation, then we have for the p-value:

$$\sup_{\lambda \leq \lambda_0} \mathbb{P}_\lambda(X \geq t) = \sum_{k=t}^{\infty} \frac{\lambda_0^k}{k!} e^{-\lambda_0} = 1 - \sum_{k=0}^{t-1} \frac{\lambda_0^k}{k!} e^{-\lambda_0}.$$

t-Test

This test is used to check whether the mean from a sample differs from a given value. It is based on the Student's t-distribution and from there the name of the test originates. Let $X_1, \ldots, X_n$ be a sample from a Normal distribution, where parameters μ and σ are unknown. We want to test the null hypothesis $H_0 : \mu \leq \mu_0$ against $H_1 : \mu > \mu_0$, where μ_0 is a fixed. Then we can define as test statistic [5]:

$$T = \sqrt{n} \frac{\bar{X} - \mu_0}{S_X}.$$

where $\bar{X}$ denotes the mean of X and S_X denotes the standard deviation of the sample. We will reject the null hypothesis for large values of T. This statistic T has a Student's t-distribution with n-1 degrees of freedom. For the interested reader, a proof of $T \sim t_{n-1}$ can be found in [5] under theorem 4.29. Thus cumulative density function (cdf) can be used to determine the p-value. It can be shown that the t-test is uniformly the most powerful within the class of all unbiased tests [5].

Wilcoxon signed-rank test

The Wilcoxon signed is a distribution-free test, which means hardly any assumptions are made on the distribution [5]. Thus it works for a wide variety of distributions, but at the expense of the power function of the test. It was first introduced by F. Wilcoxon in 1945 [6].The test is defined for the following situation:

Given the samples $X_1, \ldots, X_n$ and $Y_1, \ldots, Y_n$ of equal size, where X_i and Y_i for $i \in \{1, \ldots, n\}$ are paired. We want to test the null hypothesis H_0 : *The two samples come from the same distribution* against H_1 : *The first sample comes from a stochastically larger distribution than the second* [5].

If Y_i for $i \in \{1, \ldots, n\}$ is chosen to be a constant say k, we could consider that this gives an indication whether the sample of X_i for $i \in \{1, \ldots, n\}$ is usually larger than k.

Before the test statistic W can be computed, the following steps are performed.

First the $|X_i - Y_i|$ and $\text{sign}(X_i - Y_i)$ for $i \in \{1, \ldots, n\}$ is calculated, where we the $\text{sign}(x)$=0 if $x \leq 0$ and $\text{sign}(x)$=1 otherwise. In this implementation zero-differences will be excluded from the test, thus assume that we have m non-zero difference pairs left. As it will be used in the modelling to compare a real-valued number with some decimals with an integer value, this difference will never be zero. Next the pairs $|X_i - Y_i|$ for $i \in \{1, \ldots, m\}$ are ordered from smallest to largest value.

These values are then ranked where the smallest value receives 1 and the largest m, the ranking starts with the smallest value. However it might happen that r pairs have the same absolute difference, in this case the ranks of the next r positions are averaged and each pair gets this average value assigned. Thus it could occur that first smallest value in the rank list is actually ranked higher than 1, whilst the largest value is ranked is less than n. The rank of a pair $|X_i - Y_i|$ will be denoted by R_i.

The test statistic W is then defined as:

$$W = \sum_{i=1}^{m} R_i \cdot \text{sign}(X_i - Y_i).$$

So we would expect $W \approx 0$ under the null hypothesis, while high values of W would favour the alternative hypothesis. The critical values of W have been tabulated for different levels of significance [5]. The same holds for the exact p-values. For large sample sizes (from around $n \approx 20$) these values can also be approximated with the Normal distribution.

Note that there exist a couple of implementations of the Wilcoxon test. In this report we will however only use the one discussed in the previous part, which is already implemented in the SciPy package in Python.

Example, We will apply the Wilcoxon signed rank test to (X_1; X_2; X_3; X_4)=(6; 7; 8; 7) and (Y_1; Y_2; Y_3; Y_4)=(6; 8; 6; 6). Here we use vector notation just for the sake of brevity.

Let $\vec{X}$=(X_1; X_2; X_3; X_4) be (6; 7; 8; 7) and let $\vec{Y}$=(Y_1; Y_2; Y_3; Y_4) be (6; 8; 6; 6). Then the absolute differences are $|\vec{X} - \vec{Y}|$:=($|X_1 - Y_1|$; $|X_2 - Y_2|$; $|X_3 - Y_3|$; $|X_4 - Y_4|$)=(0; 1; 2; 1) and the signs are sign($\vec{X} - \vec{Y}$):=(sign($X_1 - Y_1$); sign($X_2 - Y_2$); sign($X_3 - Y_3$); sign($X_4 - Y_4$))=(0; 0; 1; 1).

Next the zero difference is deleted, so we are left with$|\vec{Y} - \vec{X}|$=(1; 2; 1) for the absolute differences and sign($\vec{X} - \vec{Y}$)=(0,1,1) for the signs.

We need to distribute the ranks 1 to 3. Since the there are two differences values with 1, both get rank (1+2)/2 = 1.5 and the value gets assigned rank 3. So the ranks are $\vec{R}$=(R_1; R_2; R_3)=(1.5; 3; 1.5).

Thus the test statistic $W = (1.5 \cdot 0) + (3 \cdot 1) + (1.5 \cdot 1) = 4.5$, this gives a p-value $p \approx 0,2$. So if the level of significance is lower than this p-value, than the null hypothesis is rejected for the alternative.

2.4 NV center

Before discussing the material, I want to stress that the following section was heavily influenced by Norbert Kalb's "Diamond-Based Quantum Networks with Multi-Qubit Nodes" [1].

There is a wide variety of optically active defects present in diamond crystal lattice, more than 100 colour centers have been observed and a significant portion has been investigated [7]. In this project only the Nitrogen Vacancy (NV) center will be considered. This defect occurs when in the lattice two neighbouring carbon atoms are replaced by a nitrogen atom and a vacant lattice site, this can be seen in Fig.2. The NV center exists in two charge states namely NV^0 and NV^-. The electronic wave function of the neutral NV^0 state is comprised of five electrons, two from the nitrogen atom and three from the carbon atoms adjacent to the vacancy. We will mainly consider NV^-, where an additional electron from the environment is captured, for example by some nearby charge traps [1].

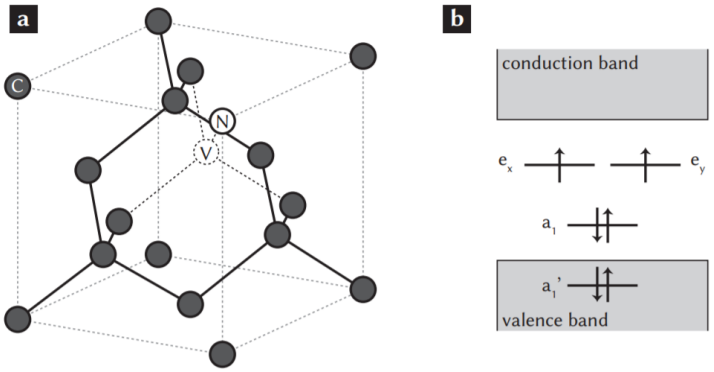

Figure 2: **(a)** The NV center is shown in the crystal lattice of diamond. The defect is formed by a substituting a nitrogen atom (N) and a vacant (V) lattice site adjacent to nitrogen for usual carbon atoms. **(b)** The molecular orbitals for the NV center are shown. The figure is taken from: [18].

The molecular orbitals can be used described to the level structure of NV^- and NV^0 as in Fig.2 [1]. These orbitals are in turn constructed by linear combinations of the dangling sp^3 orbitals, which are associated the unsatisfied bonds of the atoms neighbouring to the vacancy by considering the C_{3v} symmetry of the NV center [8]. It turns out that the ground state and the first optically excited state both only have unoccupied energy levels, which lie within the band gap of diamond [1]. Such a configuration impedes electron being lost to the conduction band as well as electron being accumulated from the valence band. Therefore NV^- has optical properties that are comparable to the properties of an individual trapped ion [10].

The ground state of NV^0 has an electron spin angular momentum $S = 1/2$, which is a singlet. On the other hand it has been shown that the negatively charged NV^- has a ground state with electron spin angular momentum $S = 1$, which is a triplet. This is consistent with having respectively an uneven and an even number of electrons surrounding the vacancy for the NV^0 and NV^- respectively [15].

When a combination of spin-spin interaction, spin-orbit interaction and Coulomb repulsion between the six electrons within the NV^- defect is regarded, it gives that the ground state is in an orbital-singlet and a spin-triplet [11]. This ground state is optically coupled to the excited state, which a orbital-doublet spin-triplet state [1], see Fig.3. From the excited state decay occurs to an intermediate spin-singlet states, from which it can decay further to the ground-state triplet that is most favourable for the state with $m_s = 0$ spin projection [1].

Electronic level structure

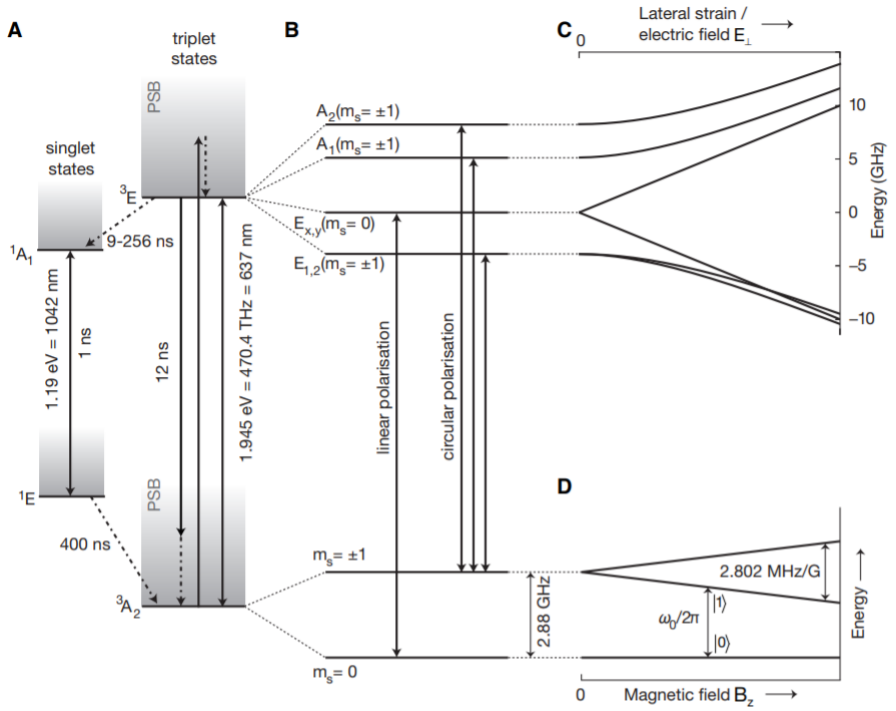

Figure 3: The electronic level structure of NV^- is shown. **(A)**: If the excitation and emission within the spin-triplet state $^3A_2 \leftrightarrow {}^3E$ occurs resonantly, no additional phonons are need [1]. This gives the zero-phonon line (ZPL). The excitation and emission can also occur off-resonantly via the phonon sideband (PSB), which is depicted by the dashed arrows. The durations of the decay times have been specified for the low-temperature-low-strain regime ($T \approx 4$ K and $E_\perp < 3$ GHz) [1]. The fact that there are state-dependent decays of ^{3}E to the spin-singlet level $^1A_1$ are present, results in varying decay rates [1]. **(B)** The spin states of the ground state of $^3A_2$ are split into two levels, where the $m_s = \pm 1$ has double degeneracy [18]. The excited state ^{3}E is divided by spin-spin and spin-orbit interactions into four energy levels, of which $E_{1,2}$ and $E_{x,y}$ are doubly degenerate [20]. The transitions from the ground to the excited states are spin selective[1]. **(C)** The effect of applied lateral strain and electric field on the energy of ^{3}E is very comparable up to first order [14]. The ground state experiences these shifts with strain and electric field very weakly [9]. **(D)** By applying a magnetic field along the axis of the NV defect the degeneracy of $m_s = +1$ and $m_s = 1$ can be lifted using the Zeeman effect. With this the states become individual addressable and this permits the definition of a qubit within the ground state triplet $^3A_2$ [1]. The figure is taken from: [1].

The zero-phonon line (ZPL) has the shape of an Lorentzian distribution (also called the Cauchy distribution) with the Half-Width Half-Maximum (HWHM) at 13 MHz for very low temperatures ($\sim$ 10 K) [12],[13]. This linewidth is fundamentally limited by the spontaneous emission lifetime of the excited states of 11.5 ns [14]. The emission spectrum of the NV center can be found in Appendix C.

Transition between charge states

The charge state NV^- is sometimes converted NV^0 [17]. This happens due to two-photon absorption. The first photon excites the electron of an NV^- to the excited state, where a second photon ionizes the electron to the conduction band. The NV center will become NV^0 either directly or through the excited state and the following fast decay. There is a similar recombination process, which turns NV^0 into NV^-. First the electron in the ground state of NV^0. Next an electron from the valence band is captured, which could have been ionized using a photon.

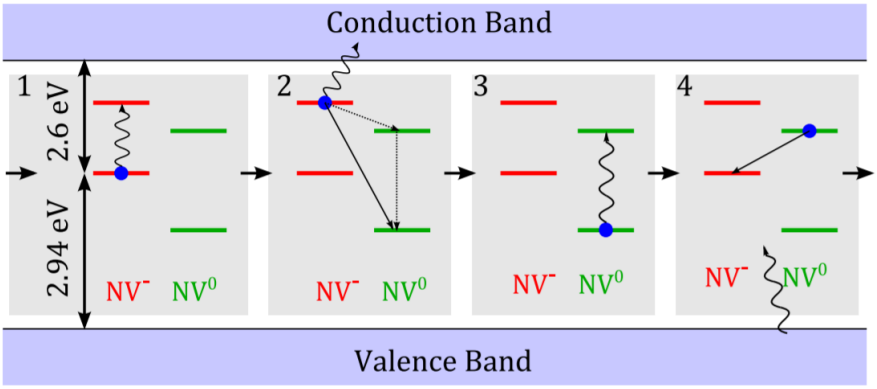

Figure 4: The mechanism of conversion of the the charge state is presented. Ionisation process: **(1)** A photon is excited an electron from the ground state of the NV^- to the by one photon. **(2)** A second photon excites the electron from the excited state of NV^- into the conduction band. Thereby the defect becomes NV^0 in the ground state, either directly after the ionization or possibly via the excited state and subsequent fast decay. Recombination process: **(3)** An electron of the ground state of NV^0 is excited. **(4)** An electron is captured from the valence band, forming NV^- in the ground state. The figure is taken from: [17].

Charge and Resonance Check

In experiments individual NV centers have to be addressed reliably and repeatedly with lasers¡ but to do this effectively there are two obstacles that must be overcome [1]. First it needs to be verified that the NV center is the NV charge state, since NV is occasionally transformed into NV^0 during experiments by the two-photon absorption process [17]. Second the optical transition frequencies are modified by fluctuations in the local charge environment. This leads to varying resonance conditions that are of hindrance for the generation of remote NV-NV entanglement, since indistinguishable emission from both emitters is needed [19].

A routine that checks both requirements has been implemented, it is called the Charge Resonance Check (CR-Check). It excites the NV with a laser set to the expected resonance frequency and counts the amount of detected fluorescence photons. If the charge state is NV^0 rather than NV^-, then the lasers are so far of resonance as the ZPL that no photons are detected at all, as the ZPL of NV^- significantly differs from the ZPL of NV^0. Otherwise a reasonable amount (around 30) photons are detected.

The linewidths of the laser that are far below the lifetime-limited linewidth of the NV center and intensities of the laser that are far below the saturation power have to be used, as this provides the maximum sensitivity with regards to the spectral diffusion [1]. The time spent in the CR-Checking process on collecting a sufficient amount of photons for verification (50 µs) is short in comparison to typical timescales for not well addressed samples (minutes or larger) [1]. The laser frequencies are chosen such that no dark state occurs, this gives a high fluorescence signal. The lack of a dark state means that each state of the ground state triplet is independently coupled to an optically excited state[1].

The experiment is started after a predefined threshold has been transcended, which is chosen such that lasers are sufficiently on resonance.

Important parameters in this CR-Check are the spectral diffusion of the NV-center and the length of the measurement time. Moreover the performance of an experiment after the passing of the CR-Check has a an effect, as it can disturb the local charge environment.

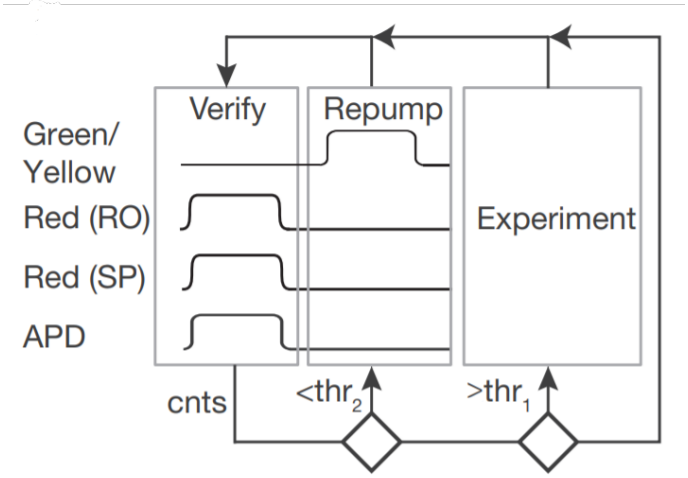

Figure 5: Graphical representation of the routine in combination with an experiment. The number of photons is counted while the NV center is excited by the Read Out (RO) and Spin Pump (SP) lasers. This is called the verification step. If the counts (cnts) exceeded the threshold for success (thr_1), then the experiment is started and the loop returns to the verification step. If the counts are below the threshold for repump (thr_2), then the repump procedure is applied and the loop goes back to the verification step. Otherwise if the counts are neither higher than thr_1 and neither lower than thr_2, then the loop immediately goes back to the verification step. The figure is adapted from: [1].

There are two methods which can be applied to return the defect into the NV^- charge state.

The most common method is to use intense (tens of µW) green laser pulses ($\lambda = 532nm$) [1]. The probability of finding the NV center in NV^- afterwards, is about 75% [17]. Moreover this intense green illumination rearranges the charge environment [1]. This can be viewed as the local charge environment being shaken up by the laser and reordered in another fashion, thus gaining a new resonance frequency. However this process also broadens the optical transitions inhomogeneously [16]. Next a verification procedure is applied to select the optical configurations that are sufficiently close to optimal. This implementation is convenient, since no feedback on the emission frequency is necessary [1].

There are some drawbacks to this method. The excessive use of these short green laser pulses can induce some slowly-decaying dynamics in the charge environment. These in turn widen the spectral emission of the NV center and such widening is detrimental as it is a hindrance to the fidelity of remote entangled states [18]. Moreover the optical transmission frequencies are less effectively tuned by the DC Stark effect in this arrangement due to screening effects, which in turn require fast switching of the applied DC voltages [22].

The alternative method is to use weak (tens of nW) and long (300 µs) yellow ($\lambda \approx 575nm$) laser pulses to reinitialize the charge state by resonantly exciting NV^0 [1]. This technique provides deterministic charge state initialization and improved spectral properties of the emission [21]. Although this procedure is in a large part free from inhomogeneous broadening of the NV emission, it requires a more sophisticated experimental control to keep the system on resonance [1]. The control loop uses a PID (proportional–integral–derivative) feedback to tune the frequencies of the applies lasers as well as the applied DC Stark-shifting which can be used to moderate small amplitude spectral diffusion [22]. This method however, will not be used in our simulation.

Due to a rapid changes in optical transitions it happens that all resonant signal is lost from the NV center [1]. Then a wide-frequency-range (about 200 MHz) automated search algorithm is applied to bring the system back on resonance [23]. The frequency and magnitude of these disruptions appear to vary for each NV center. It is hypothesized that these jumps in frequency originate from the discrete population dynamics of nearby charge traps that alter the electric field at the position of the NV dramatically due to their vicinity [1].

In our model we will only use the green laser to repump. This means that if all resonant signal is lost, green laser pulses will be applied to the NV center until it recovers resonance.

3 Algorithm

In this chapter it is discussed how the model is built up. First the most fundamental building blocks of the CR-Check will be presented and their physical meaning will be discussed. Thereafter we consider a rudimentary version of the CR-Check, which will be used to show the plausibility of the simulation. Next we elaborate on the extended routine, which is currently used in the laboratory. Following this, is a demonstration of how we obtain the optimal values for the thresholds. Thereafter the values of the variables, which will be used in the simulations, are provided.

A discussion on how the code is streamlined with regards to running time is given in Appendix D.

3.1 Fundamental functions

In this section, functions that have been specifically defined for the simulation will be discussed. First graphical representation of the standard procedure is shown where exactly these functions are applied in the procedure.

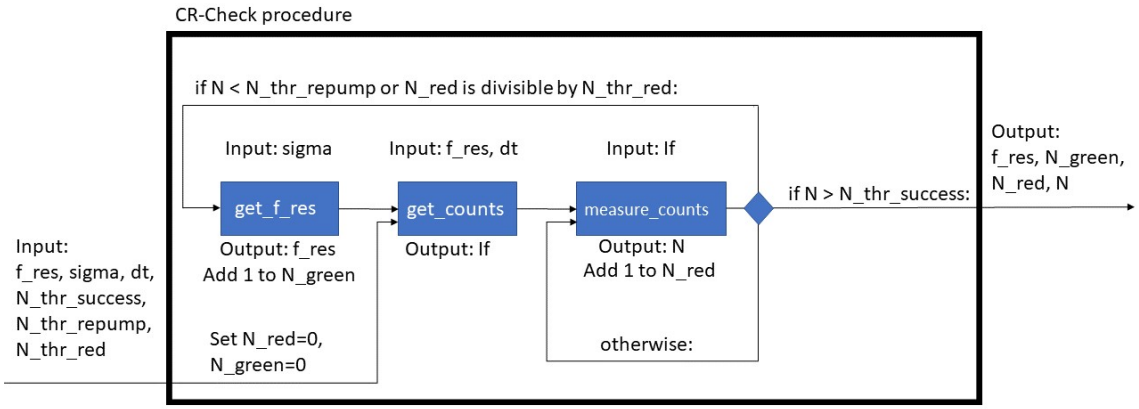

Figure 6: Visualisation of the standard procedure for the CR-Check. In the figure f_res is the resonance frequency of that particular NV center, sigma is the spectral diffusion of the NV center and dt denotes the duration of the read-out (red) laser. N_red and N_green are respectively the amount of times the functions measure_counts and get_f_res are applied. N_thr_success, N_thr_repump and N_thr_red are the thresholds for passing the test, starting the repump procedure and the maximal amount of successive read-out respectively. The average number of counts for a certain duration of the read-out is denoted by If, while N denotes the actual measured counts.

get_f_res

This function is used to determine a (new) resonance frequency for the NV center. This frequency is generated randomly from Normal distribution with mean f_red and sigma as standard deviation. The f_red is the mean of frequency of the red (read-out) laser, while sigma represents spectral diffusion of that particular NV center. This spectral diffusion stems from the distribution of the charge in the environment. In this manner the distribution of resonance frequency is symmetrical around the mean value, which we would expect for randomly chosen charge environments. This is how it is implemented:

```
def get_f_res(sigma=sigma,f_red=f_red):
    return np.random.normal(f_red,sigma)
```

Figure 7: Implementation of get_f_res.

We can regard that this function simulates when the NV center is bombarded with intense and short green laser pulses, which shake up the whole charge environment. The new charge distribution results in a new resonance frequency. As mentioned before, the excessive use of these short green laser pulses can induce some slowly-decaying dynamics in the charge environment [18]. These broaden the spectral emission of the NV center and thus perturb the fidelity of the entangled states. These effects will be simulated to some degree with the use of the memory effect.

Memory effect

We would expect there to be some memory in the system. Namely, after the NV center has passed the CR-Check routine, it should immediately afterwards pass a new CR-Check again with a high probability. The get_f_res function will also be used to model this influence of performing an experiment after successfully passing the CR-Check. However to be absolutely clear it is just used as a Normal distribution, it does not represent anymore shaking up charge environment by the green laser. Now it represents slow drifts that are modelled as steps from the current resonance frequency of the NV center. The resonance frequency f_res for the next iteration is be obtained by applying the function get_f_res to the resonance frequency of the previous iteration. The parameters given to the get_f_res function are the previous resonance frequency as f_red and the psi×sigma as the sigma. Thus we model the influence of doing an experiment as a shift from the previous resonance frequency on success.

We can immediately see that psi is somewhere in the range of 0 and 1. If psi were to be 0, then after the first time of passing, you would be immensely likely to pass all the iterations afterwards as nothing changes to the resonance frequency after an iteration. On the other hand if psi were to be 1, then we would get even more off-resonant values than with the usual f_red as mean.

As the real value of psi is unknown, we will have to determine a reasonable value experimentally. This will be done using a 2D parameter sweep of psi and sigma, where we can see the behavior of the of these parameters as this is in the end one of the main results of this work.

get_counts

Once the resonance frequency of a NV center is knows, it is used to determine the average intensity of photons coming from the ZPL. The ZPL has a Lorentzian shape [14] around median f_resonance, which is the resonance frequency of the NV center, and the scale parameter is the Half-Width Half-Maximum (HWHM). The probability density function (pdf) of the Lorentzian is translated and scaled accordingly, such that it can be used to determine the average intensity of photons. To get the average number of photons the value of pdf at the resonance frequency of the NV center is multiplied by the length of the red laser dt and a factor N_tot. We have imposed that thus the average number of photons scales linearly with dt, which is very reasonable according to what has been observed in the laboratory. The multiplication with the N_tot is used to scale intensity to the right order of magnitude, which is around 30. One could imagine that this N_tot would depend on the power of the laser, however in our model's we will not take this into account. It's sole purpose will be the order of magnitude. The implementation is as following:

```
def get_counts(f_resonance,dt=dt):
    return dt*N_tot*lorentzian(f_red,f_resonance,LL_linewidth)
```

Figure 8: Implementation of get_counts.

measure_counts

The Poisson distribution can be used to can be used to simulate a measurement of the number of photons due to the read out laser. The mean rate is obtained with the get_counts function. Now the Poisson distribution is particularly applicable here since, there is a constant mean rate and the next measurement is independent of the previous instance. Here is how it is implemented:

```
def measure_counts(N_fotons):
    return np.random.poisson(N_fotons)
```

Figure 9: Implementation of measure_counts.

3.2 Rudimentary implementation

To make the standard model credible, we started with a simplified version of the CR-Check. The code is shown below;

```
def CRcheck_prim(N_thr_success=N_thr_success,N_thr_repump=N_thr_repump,sigma=sigma,dt=dt,f_res=get_f_res()):
    N_green=0
    N_red=0
    If=get_counts(f_res,dt)
    N=measure_counts(If)
    N_red+=1
    while not N>N_thr_success:
        f_res=get_f_res(sigma)
        If=get_counts(f_res,dt)
        N_green+=1
        N=measure_counts(If)
        N_red+=1
    Delta=f_res-f_red
    return Delta, N_green, N_red, N, f_res
```

Figure 10: Implementation of the rudimentary version of the CR-Check.

First we have a NV center for which we do not have any information. The NV center has a certain resonance frequency, which we have called f_res. Next this f_res is used to determine the average number of photons using the get_counts function, which we call If. This If is then utilized in measure_count to obtain a certain number of counts and we define this to be N.

Now if the N_thr_success is surpassed, the current state is considered to have passed the check. However if N_thr_success is not exceeded by N, then we enter a loop until it does. In the loop we obtain a new f_res from get_f_res, this process is called "repump". Then again we apply again the get_counts function for If, which we use to get a new N from the measure_counts function. We repeat this process until N_thr_success is exceeded.

During the process N_green keeps track of how many times we repump, whilst N_red keeps track of how many times we measure the counts. It can be easily seen that these two are related by N_green=N_red-1 . Also upon passing the test the frequency of the red laser is calculated.

3.3 Standard implementation

The standard implementation is a generalization of the rudimentary implementation. A threshold for repump has been added. This means the repump does not occur always if the measured counts are below the threshold for success, rather it happens only when the measured counts are below the repump threshold. In addition a threshold to limit the amount of times that the function measure_counts can be applied consecutively without any repump. The code is shown below;

```
def CRcheck(N_thr_success=N_thr_success,N_thr_repump=N_thr_repump,sigma=sigma,dt=dt,f_res=get_f_res(),N_thr_red=20):
    N_green=0
    N_red=0
    If=get_counts(f_res,dt)
    N=measure_counts(If)
    N_red+=1
    while not N>N_thr_success:
        if N<N_thr_repump or N_red%N_thr_red==0:
            f_res=get_f_res(sigma)
            If=get_counts(f_res,dt)
            N_green+=1
        N=measure_counts(If)
        N_red+=1
    Delta=f_res-f_red
    return Delta, N_green, N_red, N, f_res
```

Figure 11: Implementation of the standard version of the CR-Check.

Again the resonance frequency, which we have called f_res, is used to determine the average

number of photons using the get_counts function, which we call If. This If is then utilized in measure_count to obtain a certain number of counts. Next the number of counts, which we defined by N, is determined by measure_counts using If.

Now if the N_thr_success is surpassed, the current state is deemed to have passed the check. However if N_thr_success is not exceeded by N, then we enter a loop until it does. In the loop N is compared to N_thr_repump. If it is lower than this threshold the repump procedure is started. A new f_res is obtained from get_f_res and subsequently a new If from the get_counts function. Next a new N from the measure_counts with the new If.

If the repump procedure is not started, then the N is measured again using measure_counts with the current If. This successive repetition of this process is restricted by N_thr_red.

This process is repeated until N_thr_success is exceeded.

During the process N_green keeps track of how many times we repump, whilst N_red keeps track of how many times we measure the counts for which respectively the green and red lasers are used. Upon passing the test the frequency of the red laser is calculated.

3.4 Finding optimal thresholds

We have implemented a 2D sweep over the thresholds for success and repump to find their optimal values. First the range over which the function searches for optimal thresholds is selected. Then the functions makes a grid of size range of N_thr_red times the range of N_thr_success. Grid points at which N_thr_red is larger than or equal to N_thr_success need no further calculation, as they are just nonsense. For the other grid points we will do a large number of iterations for which we can average the results such that we can compare them with other grid points.

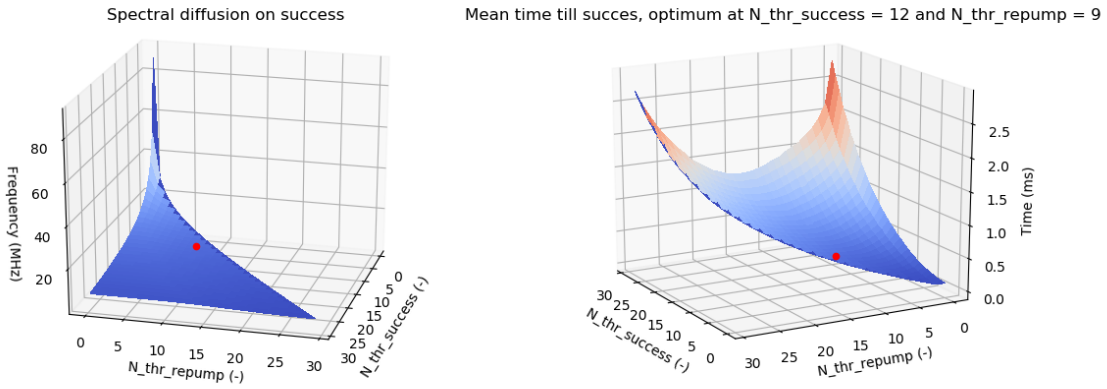

Figure 12: A visualisation of the surfaces that are calculated spectral diffusion and the mean time till success. From this the optimal values are determined. The optimal value under the given conditions is shown using the red dot.

Next the optimal values are selected in the following way. We require that the spectral diffusion is less than 11 MHZ, as we calculated the spectral diffusion as the standard deviation of the frequencies when the CR-Check was passed. This value is linked to the HWHM, but is scaled by $1/\sqrt{2\ln(2)}$ for the shape of the Normal distribution to have a more similar measure for the spectral diffusion. Subsequently from the set of grid points with spectral diffusion under 11 MHz, the grid point with the lowest mean of time till success is selected as the optimal grid point. The N_thr_red and N_thr_success for this grid point are regarded as optimal for this particular instance of the input parameters. In addition to N_thr_red and N_thr_success, the average time till success, the spectral diffusion and the value of N for which the CR-Check was passed are returned for the larger simulation.

This procedure will always be applied unless explicitly stated otherwise. From the obtained

optimal values for multiple instances, the analysis of the effects of particular parameters can be performed.

3.5 New implementations

The instances of the measured counts can also be assigned a p-value. The range thresholds for repump and success is now limited to the interval (0,1]. Moreover their definition changes, the CR-Check is passed if the p-value is less than N_thr_success, while the repump process is initiated if the p-value is higher than N_thr_red.

The code is for all these implementations with the p-value is very similar. It is basically the standard implementation of the CR-Check which is modified to handle p-values and to save the measured counts for the same resonance frequency in arrays, until the repump procedure is started. For the sake of brevity the complete code will not be presented here in full-detail, the interested reader can find a link to the code in the appendix. In the next part we will highlight the most important lines of these particular implementations, which contain how the p-value is determined for these three different statistical tests.

Using direct test

The cumulative density function of the Poisson distribution can be used to determine a set of p-values under the null hypothesis. These values can be saved in an array to be used to compare with the observation, this is much quicker than recomputing the p-value the whole time. The implementation is shown in the figure below.

```
p=Range[N]
```

Figure 13: Shows the assigning of the p-value for the direct test. The value is obtained from the Range array containing the p-values, for which the value is read out at N, the measured counts.

Using t-test

Another method is to use Student's t-test, in which the samples are Normally distributed. However we have also shown that the Poisson distribution with parameter λ goes to a $N(\lambda, \lambda)$ in distribution, as $\lambda \to \infty$, see Theorem.5. This normal approximation is already sufficient good around $\lambda \approx 20$. On the HWHM there are 18.36 counts on average, thus we can assume that the normality is adequate. We will use the standard SciPy implementation of the t-test.

```
stat,p=sp.ttest_1samp(N_arr[:i],minval)
p=p/2
```

Figure 14: Presents the calculation of the p-value for the t-test. The array containing the measured counts is denoted by N_arr. The position to which the array containing the measured counts is filled, is denoted by i. The average of the counts on the HWHM is denoted by minval. The p-value given by the SciPy function is a two sided p-value, thus it is halved.

The second line is used to make the p-value one-sided again. To be sure that the test is applied one-sided, an extra constraint has been added for the threshold for success. It requires that the mean of the first i elements of N_arr are larger than minval.

For more information on the ttest_1samp function, we refer the interested reader to the SciPy source code.

Using Wilcoxon signed-rank test

Alternatively, the Wilcoxon signed-rank test can also be used. The major advantage is that this is a distribution free test, thus no assumptions are made on the distribution of the samples. The comparison will be made between the array containing the measured counts and an array of equal size solely containing the average of the counts at the HWHM. We will use the standard SciPy implementation of the Wilcoxon. signed rank test.

```
stat,p=sp.wilcoxon(N_arr[:i],y[:i],zero_method='wilcox', alternative="greater")
```

Figure 15: Shows the calculation of the p-value for the Wilcoxon signed-rank test. The array containing the measured counts is denoted by N_arr. The position to which the array containing the measured counts is filled, is denoted by i. The other array, y, contains only the value of the counts on the HWHM. The p-value given by the SciPy function is one-sided due to the alternative="greater". The function automatically chooses whether is should use the exact form or a normal approximation.

For precise information of the wilcoxon function, we refer the intersted reader to the SciPy source code.

3.6 Variables

Now that we have established that our model works reasonably and gives a somewhat realistic simulation, we can start to scan the parameter space to understand what the effects are of different variables in the CR-Check. However there are multiple variables used in the model. The table below provides the numerical value of these variables that are used during the simulation. These values are used unless specifically stated otherwise:

Table 1: Definition, explanation and numerical value of all the variables that are used in our model.

Variable	Definition	Value
dt gauss	Duration of the repump proces (green laser)	400 µs
dt	Duration of the measurement of the count (red laser)	50 µs
sigma	Standard deviation from the average resonance frequency	50 MHz
lambda_red	Average resonance wavelength (in vacuum)	637 nm
c	Speed of light (in vacuum)	299792458 m/s
LL_linewidth	Lifetime Limited Linewidth	13 MHZ
N_tot	Multiplication factor for the Lorentzian	$0.3 \cdot 10^{14}$
psi	Memory parameter	0.2
N_thr_red	Maximal times read-out consecutively	20

It is important to mention that with these standard values, we get an average of 36.728 counts when perfectly on resonance.

The number of iterations over which we average was chosen such that the simulation speed was acceptable. The reality of the model was not generally hampered by the number of iterations as we took over 150.000 iterations per particular set of parameters. For the 1D variations we even did over 1.500.000 iterations per particular set of parameters. Thus this suggests that the Law of Large Numbers (3) and (4) will apply to this situation.

4 Results

First the results for the parameters, which will be experimentally assigned a value, are presented, as they influence all other results. Next 1D sweeps of spectral diffusion and the dt are shown. For completion the 2D has been added in Appendix, since the observations in the 1D sweeps. This is followed by the results of the other protocols.

4.1 Memory parameter

As mentioned in the section about the get_f_res function, there is a strong idea that there should be some kind of memory in the system. The implementation was also discussed there. Thus it should be more likely to pass a CR-Check again once it passed the first time. To get a good insight of what the parameter does, a 2D sweep of the memory parameter and the spectral diffusion on the standard CR_Check function for the mean time till success. Also as mentioned before, the psi parameter will be in the domain of 0 to 1, thus we will only search this part of the parameter space.

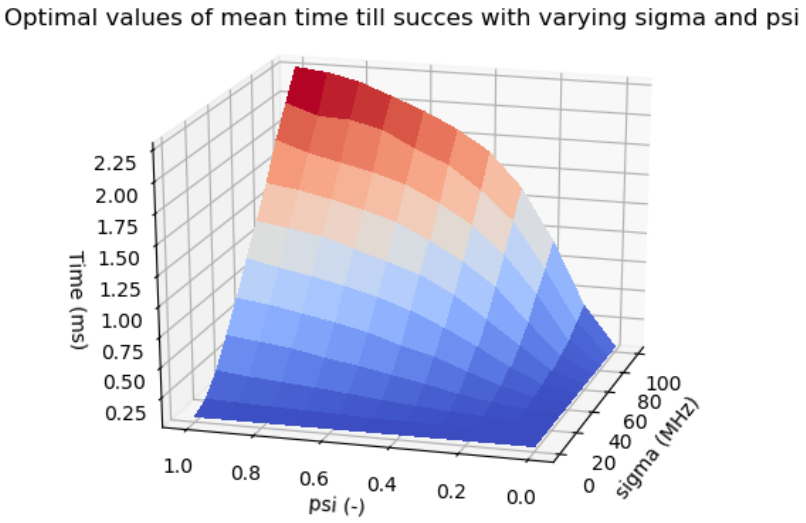

Figure 16: A visualisation of the optimal values of mean time till success for varying spectral diffusion and psi

As can be seen in figure 16, values for psi of higher than 0.5 have little influence on the mean time till success. This can be seen in particular for low values of the spectral diffusion, where we would expect a stronger effect. On the other hand if psi is 0 the memory effect is too strong and all the information is lost in the figure, as after the first instance success almost solely successes occur. But to encapsulate some memory effect in our model, the value 0.2 is chosen as a reasonable value for psi.

This psi parameter relates the spectral diffusion of the defect and the shift in resonance frequency due to an experiment. The spectral diffusion is governed by the effect of the local charge environment [15] and we believe that the psi also depends on the local charge environment. So the psi parameter depends heavily on the what occurs in NV center in between CR-Checks. On

longer timescales, this drifts dependence on other parameters might start dominating the drift, as these parameters also drift themselves. We hypothesize that such parameters are the NV center's temperature (if it is not cooled continuously) and the electromagnetic fields of the lasers. The shielding effect might have an influence as well, it can be induced by a large amount of repumps.

If nothing would permute the local charge environment, then a perfect memory could be expected. This is for example the case if a CR-Check is started immediately after the previous has been passed. On the other hand if the local charge environment changes due to a measurement, the psi parameter would be measurement specific. This is all because the fluctuations in the local charge environment are contingent on the measuring procedure. Therefore it is hard to assign a proper value to the psi parameter.

4.2 N_thr_red parameter

This N_thr_red was first introduced to prevent an infinite loop if the thresholds for success and repump are far apart and it was therefore set to 100. It limits the amount of times that the read out laser can be used consecutively, without repumping. However it can also be employed as a parameter, as it could be faster to require a repump after a certain amount of read-outs. This parameter might be dependent on the spectral diffusion, and that is why a 2D sweep over sigma and N_thr_red is used. We obtained the following results.

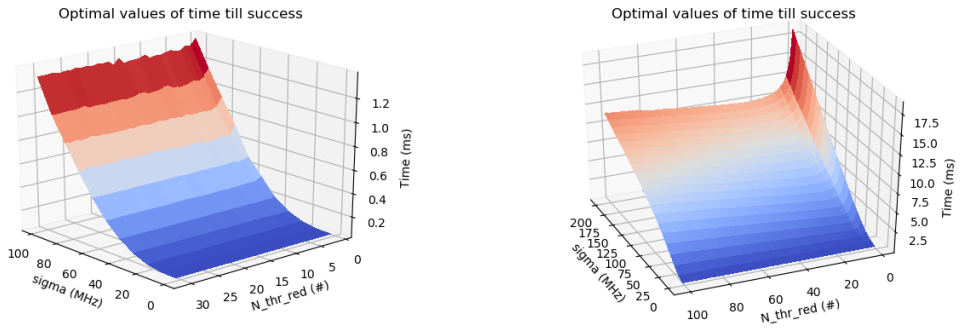

(a) Plot of the the mean time till success over varying sigma and N_thr_red, where we always take the optimal value for N_thr_success and N_thr_repump.

(b) Plot of the the mean time till success over varying sigma and N_thr_red, with fixed thresholds at N_thr_success = 30 and N_thr_repump = 3.

Figure 17: The results of the variation of N_thr_red and sigma.

As we see in Fig.17a N_thr_red does not have a significant influence, if it is chosen to be sufficiently large (i.e. larger than 10). When we fix the thresholds of success and repump at a far apart from each other, we get Fig.17b. Here an optimum is present and it seems that the optimum is dependent on sigma.

The value of N_thr_red will be set to 20 for the other variations.

4.3 Distribution of frequencies

It is very illustrative to see what kind of distribution is obtained for the distance between the frequency of the red laser (λ = 637 nm) and the resonance frequency of the NV center upon passing the CR-Check.

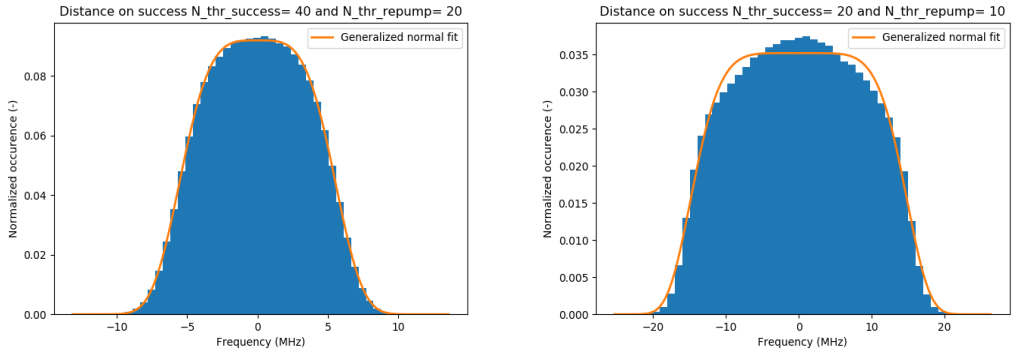

(a) Histogram of the distance in frequency upon passing the CR-Check for values N_thr_success = 40 and N_thr_repump = 20. The Generalized Normal is fitted, the fitted parameters are $\mu = -0.00563$ MHz, $\beta = 3.90$ and $\alpha = 6.01$ MHz.

(b) Histogram of the distance in frequency upon passing the CR-Check for values N_thr_success = 20 and N_thr_repump = 15. The Generalized Normal distribution is fitted, the fitted parameters are $\mu = 0.00161$ MHz, $\beta = 5.79$ and $\alpha = 15.3$ MHz.

Figure 18: The distributions of the distance in frequency upon passing the CR-Check, with the standard values of dt = 50 µs and sigma = 50 MHz. Note that these are generated for fixed values of N_thr_success and N_thr_repump, so the standard optimization for the thresholds has not been applied.

As can be seen in Fig.18a, the generalized normal seems to be the distribution of the frequency after passing the test. However due to the memory parameter, this distribution is altered in particular when N_thr_success is not high (above 30) as in Fig.18b. The generalized normal is still a reasonable approximation of the distribution in this individual case, however this varies and given a value for psi it is most strongly contingent on N_thr_success and N_thr_repump.

As mentioned before, it is very important to keep the spectral diffusion below the lifetime limited linewidth to be able to generate entanglement successfully, since indistinguishable photons are needed for entanglement.

4.4 Variation of sigma

Now that the N_thr_red and psi parameters have a value assigned to them, the 1D sweeps over the spectral diffusion can be done. This is done first for a range of sigma of 0 to 200 MHz.

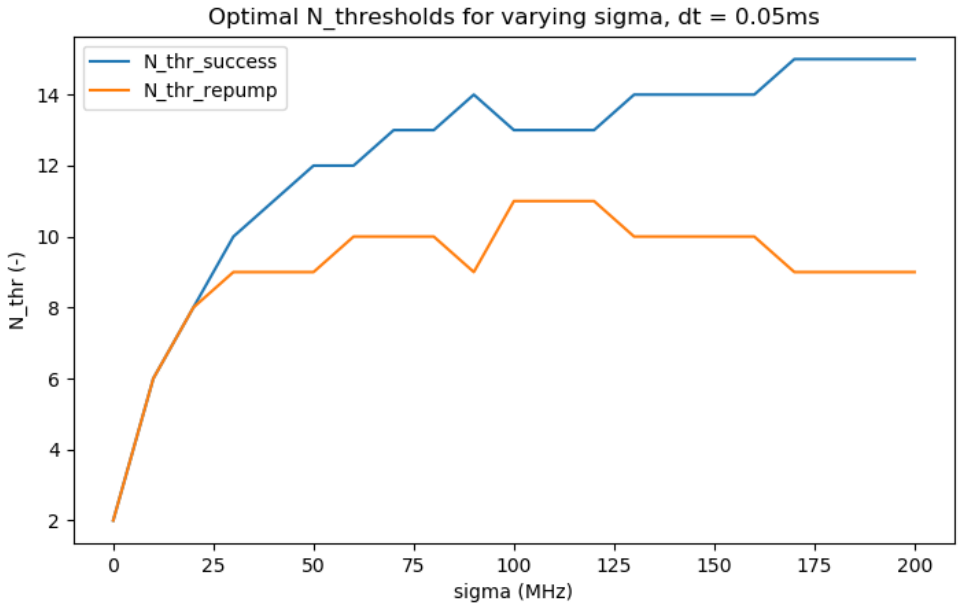

(a) Plot of the optimal values for threshold for success and the thresholds for repump over varying sigma.

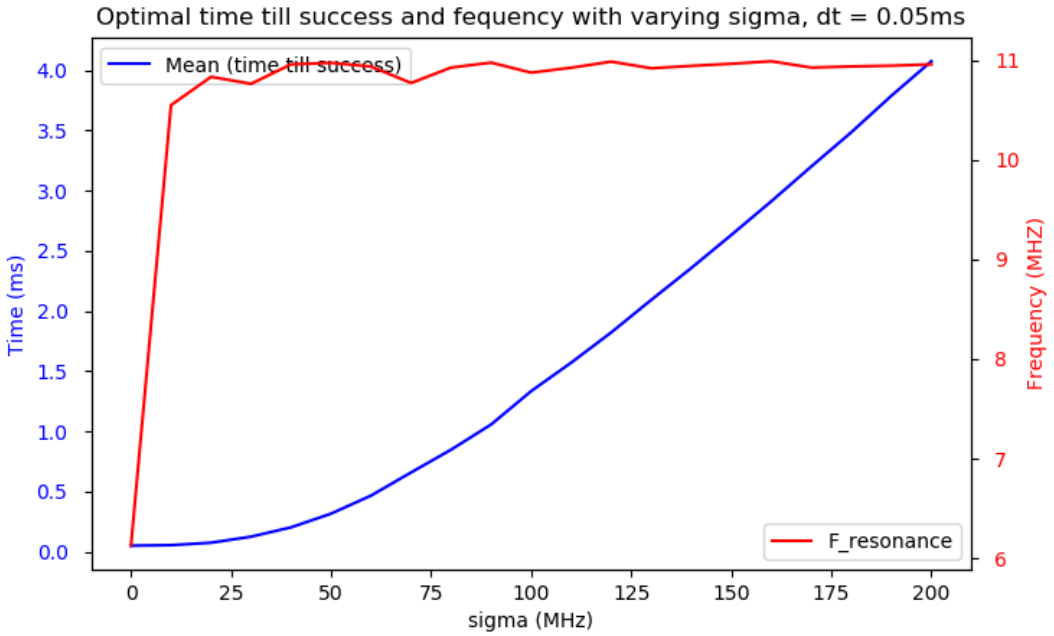

(b) Plot of the average resonance frequency on success and the mean time till success with varying spectral diffusion.

Figure 19: The results of a sigma variation from 0 to 200 MHz with dt = 50 µs.

Interesting to note is the from the figure is the dependence of the mean time till success on the spectral diffusion. First it seems that the mean time till success scales with a power of sigma, but from around 80 MHz it starts scaling linearly. This becomes particularly evident when we take a greater range of sigma from 0 to 500 MHz, this result is shown in Appendix E.

It can be observed that the thresholds for success and repump become constant after a spectral diffusion of about 200 MHz. We could see this as the worst case scenario, in which the CR-Check routine has to have the highest standards to still be sufficiently effective. The spectral diffusion does not fluctuate much after 100 MHz under the optimal values for the requirement that it is

under 11 MHz , only the mean time till success starts increasing linearly.

We can explain this scaling with sigma in the following manner. At a certain point the Normal distribution with mean f_red and variance sigma, becomes wider sigma increases. This has two consequences in a limited range around the resonance frequency, where the CR-Check comes due to the constraint on the maximal spectral diffusion. Namely it widens the top of the pdf of the distribution and it lowers the pdf. After 80 MHz, this top has become sufficiently flat such that the only effect which is noticeable becomes the lowering of the pdf. This lowering can be observed as the linear increasing mean time till success. The behavior of the scaling for the low spectral diffusion (under 50 MHz) can be attributed to the memory parameter. As it affects the mean time till success a lot, which we already observed.

The value of the laser duration can also be set to another value, to see if some differences would occur. For the next results dt was changed to 25 µs.

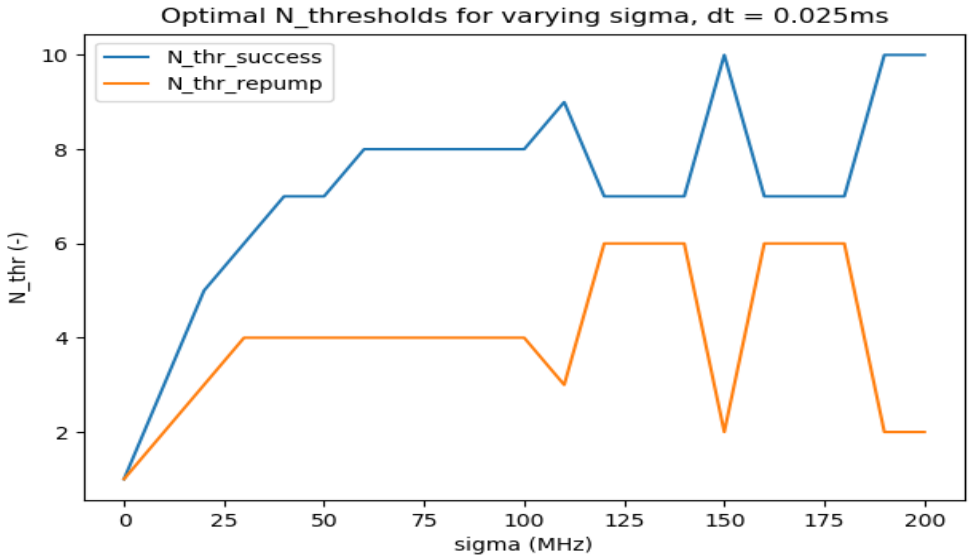

(a) Plot of the optimal values for threshold for success and the thresholds for repump over varying sigma for dt = 25 µs.

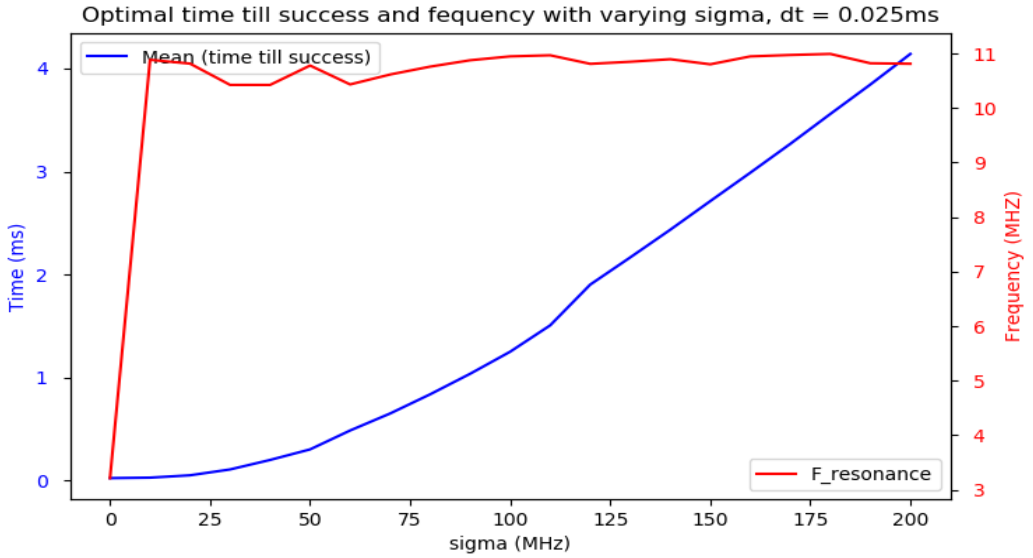

(b) Plot of the average resonance frequency on success and the mean time till success over sigma for dt = 25 µs .

Figure 20: The results of a sigma variation from 0 to 500 MHz with dt = 25 µs.

From both Fig.19a and Fig.31a, it can also be remarked that the thresholds seem to come in pairs. The changes in thresholds occur almost always simultaneously for both N_thr_success and N_thr_repump. This can be attributed to the general effects of the N_thr_success and N_thr_repump on the spectral diffusion after the CR-Check. Making N_thr_success requires thus more photon counts to be measured , this lowers the spectral diffusion after the check. On the other hand lowering N_thr_repump from the value of N_thr_success increases the spectral diffusion. From the right balance between the values of these two parameters, the optimal value for mean time till success arises. Since some combinations always result in a too high spectral diffusion, whilst other take too long. This could be the reason that these well-fitting pairs for values N_thr_success and N_thr_repump arise.

As another quality check of the routine, the average photon counts on success are presented over varying sigma.

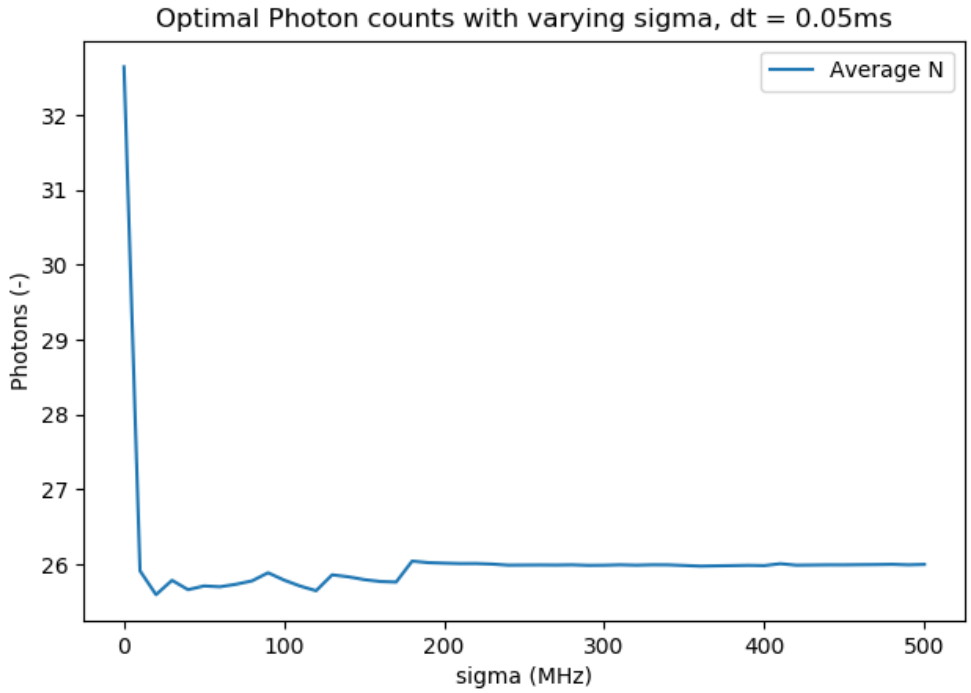

Figure 21: Plot of the average photon counts on success for the optimal values with varying spectral diffusion.

Indeed at 0 spectral diffusion we will get the highest average photon counts, since we are on resonance. But this average goes down quickly as the spectral diffusion increases. From 100 MHz of spectral diffusion and onwards, nearly the same average photon counts is present. This is a sign that the NV center is always brought sufficiently on resonance by the CR-Check routine.

Another comparison can be made with the simplified implementation of the CR-Check, without the repump threshold or one could regard that this is the case where the N_thr_success and N_thr_repump are equal to each other.

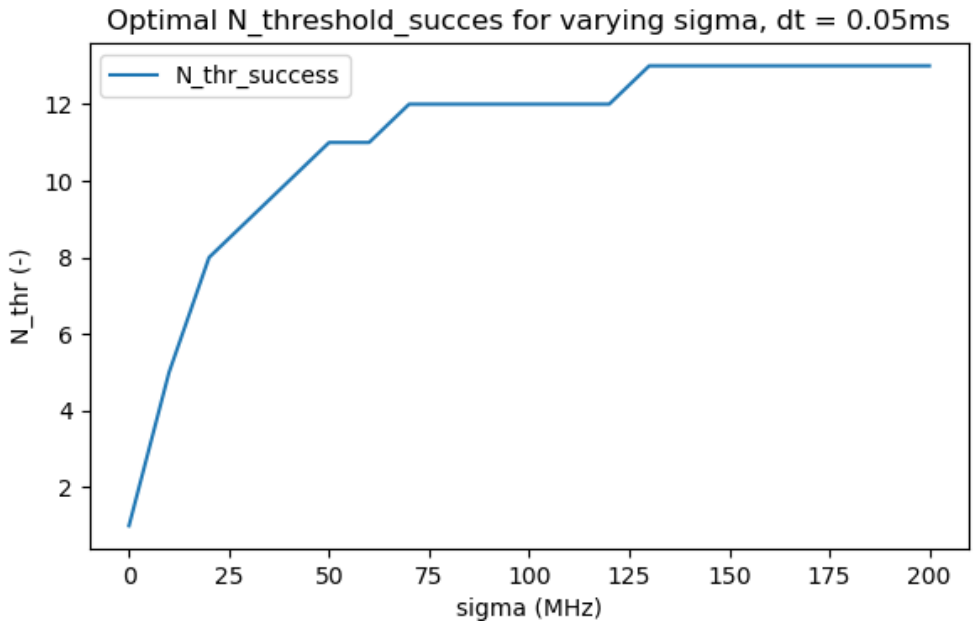

(a) Plot of the optimal values for threshold for success and the thresholds for repump over varying sigma.

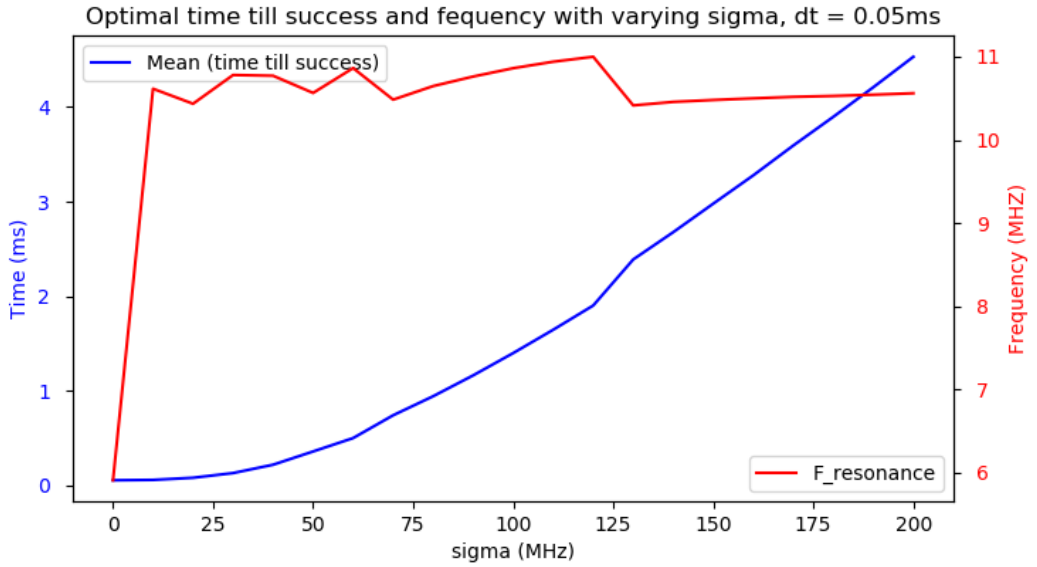

(b) Plot of the average resonance frequency on success and the mean time till success for varying spectral diffusion.

Figure 22: The results of a sigma variation from 0 to 200 MHz of CR-Check_prim algorithm with dt = 50 µs.

In Fig.22a the optimal threshold for the high values of the spectral diffusion is now 13, rather than 15 which we observed in Fig.31a. This is consistent with ideas discussed in the remarks about the pairs of thresholds. As this can be viewed as N_thr_repump being maximal, the N_thr_success can be lowered to optimize for the mean time till success on the condition that it keeps the spectral diffusion under the required maximum.

Comparing Fig.22b to Fig.19b, gives that the standard routine is already about 10% faster than the simplified version. It is not surprising that the simplified implementation is slower than the standard implementation, as it is contained in the standard implementation so it can never be faster.

4.5 Variation of dt

The natural follow up of sigma variation is to now apply 1D sweeps over the laser duration. This sweep is performed in the range of 5 to 105 µs, unless explicitly stated otherwise.

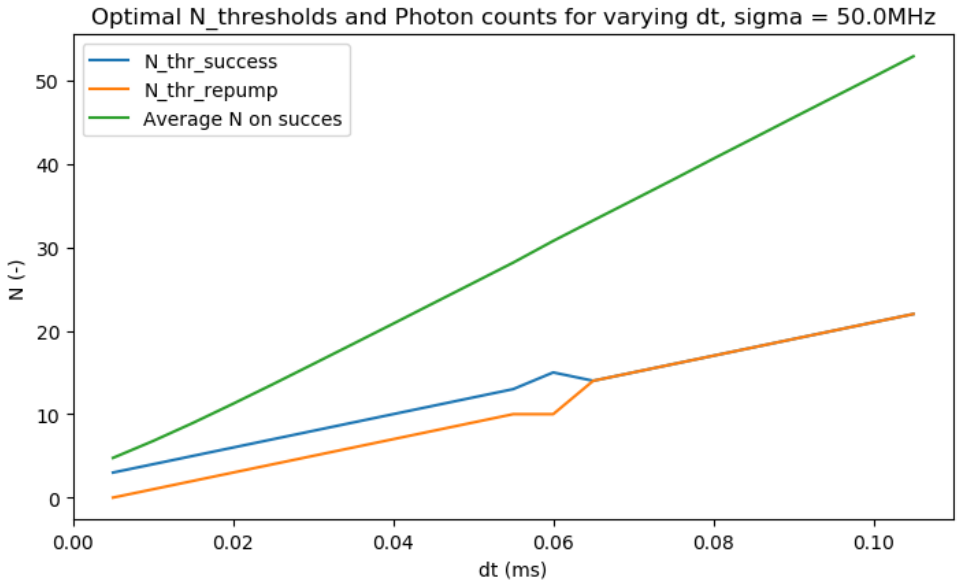

(a) Plot of the optimal values for threshold for success and the thresholds for repump over varying dt. In addition to this, the average number of counts on success is shown.

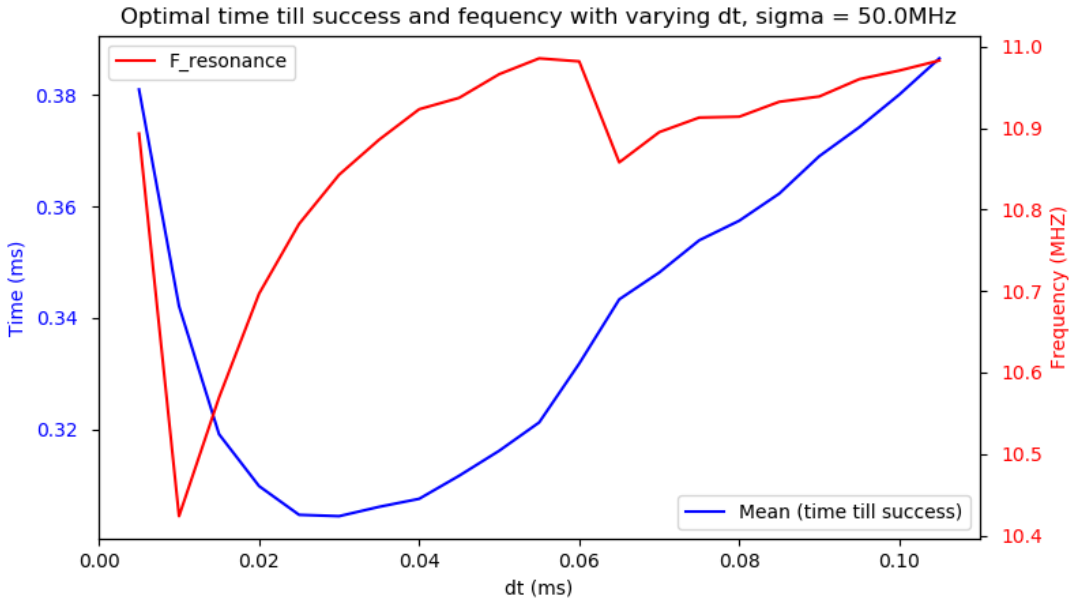

(b) Plot of the average resonance frequency on success and the mean time till success over varying dt.

Figure 23: The results of a dt variation for and sigma = 50 MHz.

It is very interesting to see that there is a clear minimum for dt=25-30 ms in Fig.23b, this suggest that there could exists a time for which the laser duration provides the highest efficiency with regards to the mean time till success for this sigma. For too low values of dt, the maximum of the average number counts on resonance is low. As a consequence, slightly off-resonant resonance frequencies, which are sufficiently good, will already have great troubles even showing any fluo-

rescence. It also becomes harder to distinguish between resonance frequencies that are sufficiently good and that are too much off-resonance, since the differences have become smaller.

In Fig.23a, it can be seen how the thresholds go up with the same linear rate, while the average number of photon counts on success increases with a faster linear rate. The rate of the thresholds has been estimated at 0.2 per µs.

Again, the existence of the pairs of the thresholds is observed. Moreover from 0.065 ms onward the thresholds are equal, this means that there is no special threshold needed for the repump procedure. This can be considered as that the difference between sufficiently and insufficiently resonant frequencies becomes large enough to differentiate between them in one measurement.

Now the spectral diffusion is set to 100 MHz rather than the usual 50 MHz. This gives the following results.

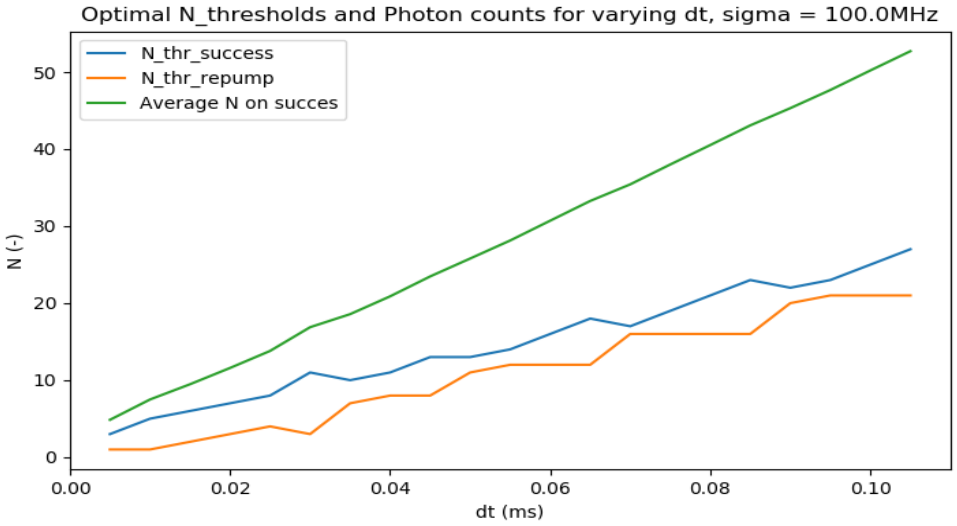

(a) Plot of the optimal values for threshold for success and the thresholds for repump over varying dt and sigma = 100 MHz. In addition to this, the average number of counts on success is shown.

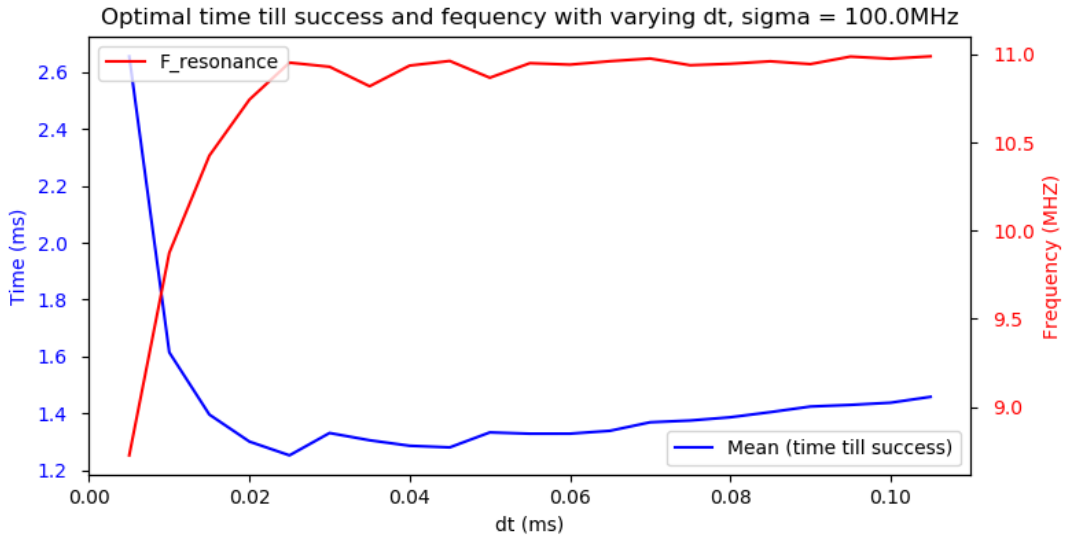

(b) Plot of the average resonance frequency on success and the mean time till success over varying dt and sigma = 100 MHz.

Figure 24: The results of a dt variation for and sigma = 100 MHz, which is twice the standard value.

Again a minimum is observed, however the shape of the mean time till success differs sig-

nificantly. We also remark that dt for the minimal time till success might be dependent on the spectral diffusion, this can be investigated further with the 2D Variation of sigma and dt. Now the thresholds do not become equal at any moment, as can be seen in Fig.24b. The rate by which they go up seems to be really similar to the one at the lower spectral diffusion. The concept that there are favourable pairs still seems to be reasonable.

Now we can again compare it with the simpler version of the CR-Check, which does not have a repump threshold. This is done in a range of 0.5-2.5 times the standard value, so from 25 to 130 µs.

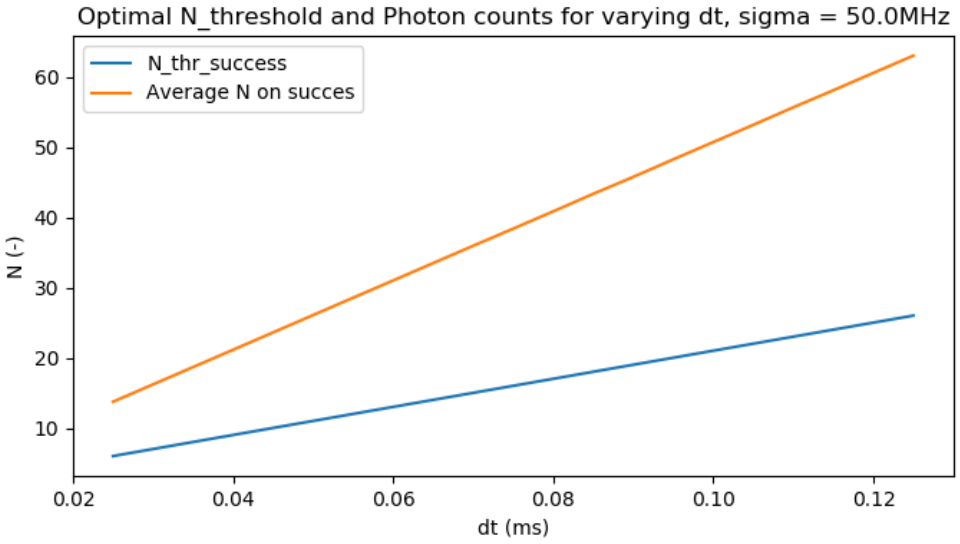

(a) Plot of the optimal values for threshold for success and the thresholds for repump over varying dt. Moreover the average number of counts on success is shown.

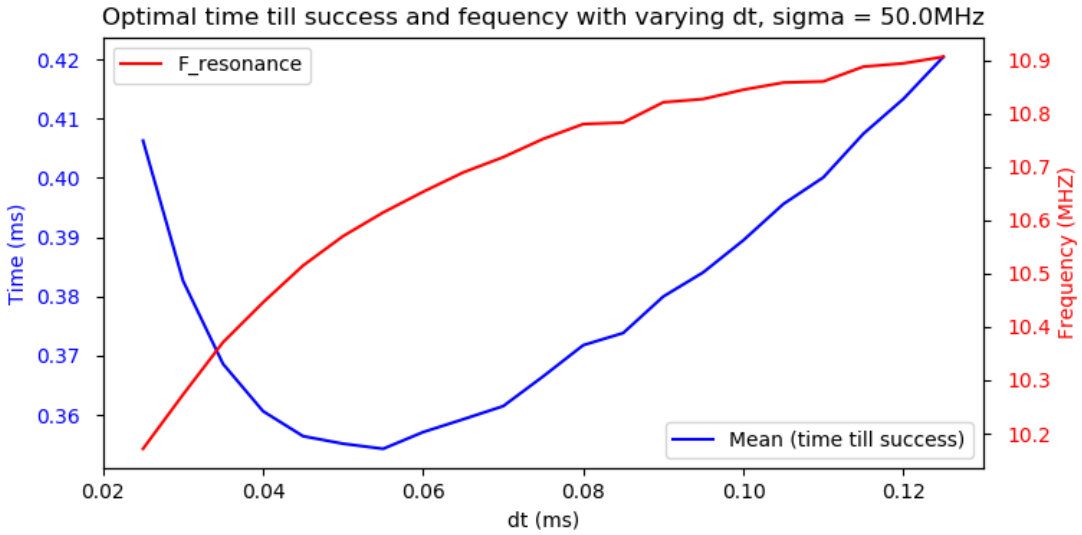

(b) Plot of the average resonance frequency on success and the mean time till success over varying dt.

Figure 25: The results of a dt variation for and sigma = 50 MHz for the CR-Check_prim implementation. The range for the dt variation is from 25 to 130 µs.

The curve in Fig.25b appears to be fairly similar to the one in Fig.23b, however it is shifted. The minimum is now around 55 µs, where it was around 25 µs in Fig.23b. So this shift might be majorly caused by the addition of the repump threshold, as that is the largest difference between the two implementations.

4.6 Comparing strategies

As we have observed in Fig. and23b in Fig.24b there seems to be an optimum around dt = 25 µs, which is half of the usual laser duration. Further investigation is performed to determine whether the standard routine with dt = 25 µs would be a quicker routine. Therefore the standard routine with dt = 50 µs is compared to the standard routine with dt = 25 µs over varying sigma. This gives the following results.

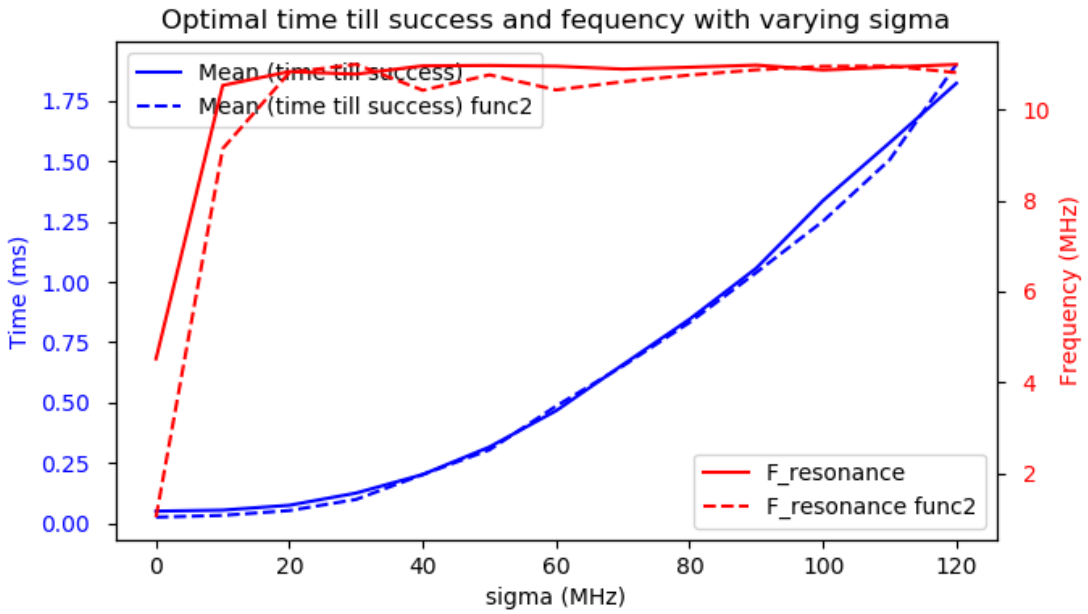

Figure 26: Plot of the average resonance frequency on success and the mean time till success with varying spectral diffusion. The full lines belong to the CR-Check with dt = 50 µs, whilst the dashes lines belong to the CR-Check with dt = 25 µs. Moreover the term func2 is used to stress that a second implementation is used.

From Fig.26, we see that for low spectral diffusion (sigma smaller than 40 MHz) the CR-Check with half dt is significantly more favourable (in relative terms) with regards to the meantime till success. Because in these iterations it seems that in the first (or first few) tries the CR-Check is already passed. This effect might also be attributed to the memory parameter, which allows for such quick passing of the CR-Check.

But in general there is very little difference between the strategies. This might the consequence of the fact that the difference between sufficiently and insufficiently resonant frequencies becomes too small to efficiently distinguish for low dt and simultaneously keep the spectral diffusion under the required 11 MHz.

4.7 New strategies

In this section the results will be given of the new implementations with the bounds on the p-value serving as the N_thr_success and N_thr_repump. First the results of the routine using calculation of the p-value with the Poisson distribution is shown. Following this are the results of the implementation with the t-test and then finally the results of the implementation with the Wilcoxon signed-rank test is presented.

Using direct test

The results of a sigma variation are shown for the direct test. In this implementation previous p-values are discarded, however in future research it might be considered to combine the p-values with the appropriate methods [25].

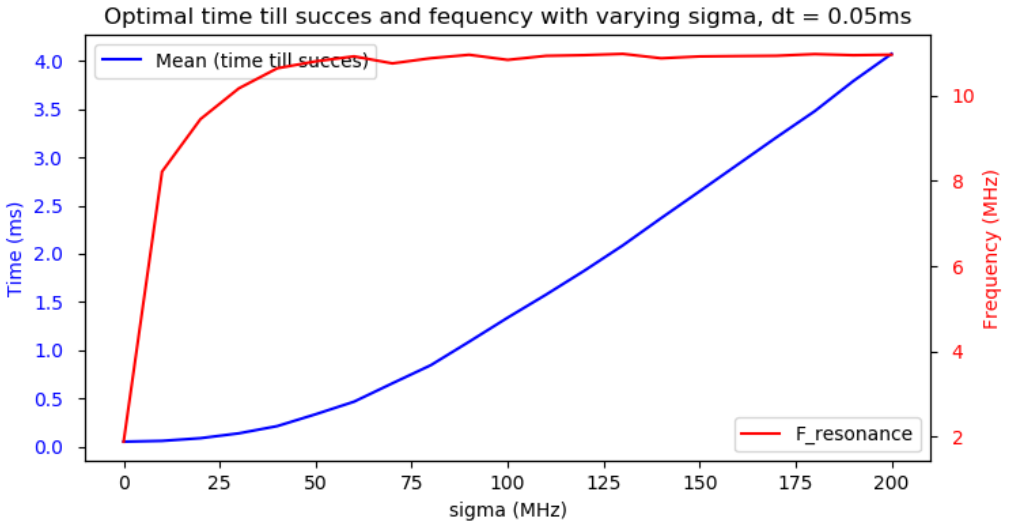

Figure 27: Plot of the average resonance frequency on success and the mean time till success over varying spectral diffusion for the direct test implementation with dt = 50 µs.

These results are very much like the usual implementation, where the amount of measured counts is directly compared with the thresholds, see Fig.19b. However in Fig.27 the of the spectral diffusion after the test increases smoother compared to Fig.19b. Considering the list for the p-values of different amounts of measured counts, we can relate the optimal bounds on p-values of N_thr_success and N_thr_repump to an amount of counts. Unlike the thresholds for direct comparison, p-values belonging to two neighbouring thresholds are not equally equidistantly separated. This explains the small difference between this implementation and the standard implementation, this difference is disadvantageous for this implementation.

Using t-test

The results of a sigma variation are presented for Student's t-test.

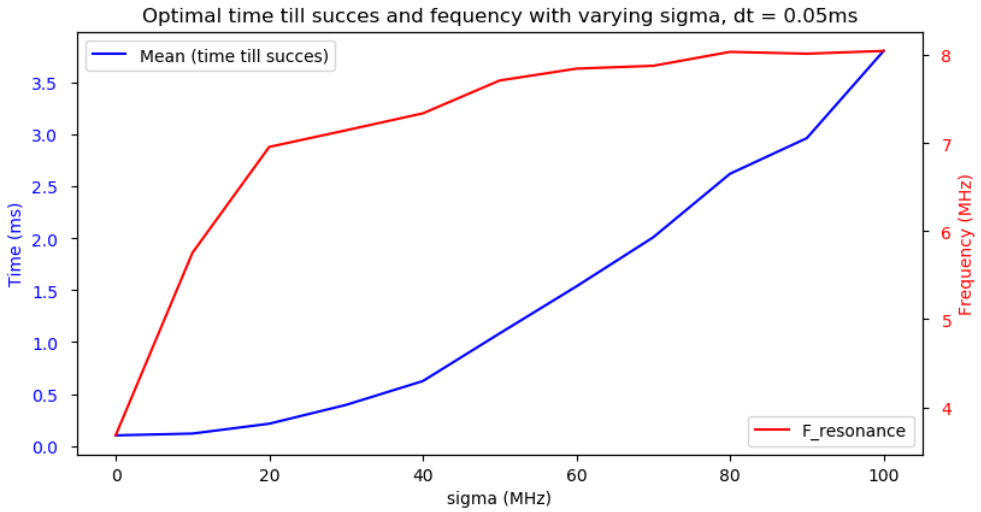

Figure 28: Plot of the average resonance frequency on success and the mean time till success over varying spectral diffusion for the t-test implementation with dt = 50 µs. Note that these values are from just 1000 iterations per instance an that N_thr_red was set to 10.

The computation time per CR-Check with this implementation is very high and therefore the

amount of iterations is significantly limited, only 1000 iterations have been performed. These results should be regarded as a proof of concept that the t-test implementation can work as a CR-Check. Moreover large trends can still be considered.

It can be observed from Fig.28 that the maximal spectral diffusion is significantly below the the 11 MHz bound. This in part with the fact that the Poisson distribution is still only rough approximated by the Normal distribution, results in significantly higher mean time till success. This suggest that either the maximally allowed average spectral diffusion should be lower or that comparing the value with the one at the HWHM with the standard implementation, is not a fair comparison to make.

We would expect this method to become better if the average amount of photon counts is increased, as then the Normality assumptions becomes more reasonable. This can be achieved by increasing dt or N_tot. N_tot can for example be increased by increasing the intensity of the red laser.

Using the Wilcoxon signed-rank test

The results of a sigma variation are presented for Wilcoxon signed-rank test.

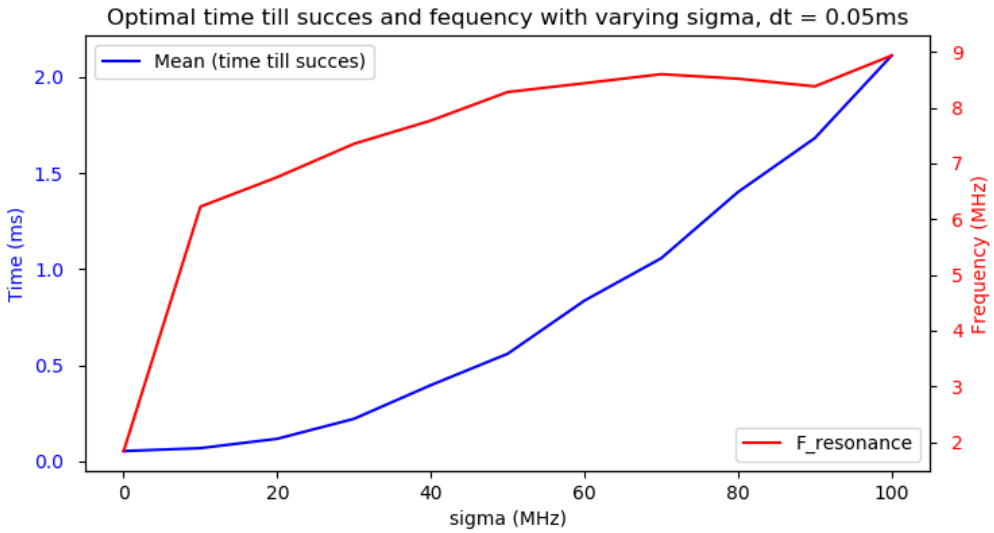

Figure 29: Plot of the average resonance frequency on success and the mean time till success over varying spectral diffusion for the Wilcoxon signed-rank test implementation with dt = 50 µs. Note that these values are from just 1000 iterations per instance an that N_thr_red was set to 10.

The computation time per CR-Check with the Wilcoxon rank test is very high and therefore again the amount of iterations done is limited considerably, only 1000 iterations have been performed. Again these results ought to be regarded as a proof of concept that the Wilcoxon sign rank test can be implemented as a CR-Check. Again the large trends can still be considered.

From Fig.29 is can be seen that the maximal spectral diffusion is significantly below the the 11 MHz bound. This results in a higher mean time till success, but not as significant as in Fig.28. However there the maximal spectral diffusion was even lower. Again the suggestion is given that either the maximally allowed average spectral diffusion should be lower or that comparing sample with the value at the HWHM with the standard implementation is not a proper comparison.

To apply this test in an experimental setup would require additional computation time compared to the standard implementation. It is fairly easy to compare two numbers with the microcontrollers, however calculating the test statistic requires more computation power. This calculation requires sorting through measured data and this is expensive with regards to the computation time. It needs to be performed before every measuremt which is in the time scale of ($\sim$ 50 µs). However the maximal amount of values to be sorted through is limited by the N_thr_red. Thus, good equipment and a quick protocol could probably suffice.

5 Conclusions

In this report a model for simulating the charge resonance Check in the NV center was created. It was used to do parameter sweeps. First the value of the memory parameter was determined experimentally with a 2D sweep of psi and sigma. It was set at 0.2 such that there is some effect noticeable. Next a 2D sweep was performed over N_thr_red and sigma. Therefrom it was concluded that for not to significantly different N_thr_repump and N_thr_success that N_thr_red just has to be chosen large enough because there was no clear minimum. N_thr_red was placed at 20.

With these values set the distribution of frequency spectrum was investigated. Without the memory parameter it follows the Generalized Normal distribution. However due to the memory parameter this Generalized Normal distribution is perturbed.

From the 1D variation of sigma, we observed that the mean time till success goes up linearly sigma after 80 MHz. This effect is attributed to looking at the Normal distribution on a finite domain for a increasing value of the variance. First the top of the pdf widens, while the whole pdf is the lowered. But after a sufficiently high variance only the lowering of the pdf is noticeable on finite domain.

For sigma higher than 180 MHz the same N_thr_repump and N_thr_success are used. This can be seen as the thresholds having the values of the worst case scenario.

Together with the 1D variation of dt it became clear that the N_thr_repump and N_thr_success often come as pairs, as they almost always change their values simultaneously. This was particularly detectable in the dt variation, where these thresholds go up at the same rate.

In the 1D variation of dt, we noticed that for fixed sigma there is a optimal value of dt. It was hypothesized that this optimal value of dt depends on sigma. A bit of this effect could be observed in the 2D variation of sigma and dt.

Particularly the plot of the optimal photon counts, i.e. the average number of photon counts upon passing the CR-Check, showed the robustness of the CR-Check. Average number of photon counts was nearly independent of sigma (if we leave out the extremely low spectral diffusion) and only linearly dependent on dt. This is a sign that the CR-Check can always bring the NV center sufficiently on resonance, The was also the 2D variation of sigma and dt.

It was shown that for sigma below 40 MHz, it is significantly faster to use the CR-strategy with dt = 25 µs compared to the standard dt of 50 µs.

In the report we used the standard deviation to quantify the spectral diffusion of the defects that passed the CR-Check. The maximal value of the average spectral diffusion was set at 11 MHz. This is the 13 MHz of the lifetime limited linewidth of the zero-phonon line, but only scaled to the HWHM of a normal distribution (which is an approximation). The suggestion arose that this value of 11 MHz is not restrictive enough.

In future research it might be interesting to do a more extensive enquiry into the best possible measure for the spectral diffusion after the passing of the CR-Check. This research will have to take the dependence of the frequency spectrum distribution on the memory parameter into account.

All the implementations with the p-values were shown to be a liable candidates to be incorporated in the procedure of a CR-Check.

The direct test functions nearly as good as the standard implementation with regards to the mean time till success, as they are very closely linked. Further investigation for direct test could be done on enhancement by combining the p-values in a fitting manner.

The implementation with Student's t-test has shown to restrict the spectral diffusion more than required, this results in a much higher mean time till success. However it also has a lot of potential for further inquiries. Firstly it is uniformly the most powerful test in the class of unbiased test. Secondly the hurdle of many additional computations to obtain the p-value can be counteracted with smart implementation. A library could be prepared of p-values for the particular values of the statistic. Let k be an integer of the highest value that will be obtained by a finite sample Poisson distribution, which is of course dependent on dt. Now the fact that the Poisson distribution gives integer values can be exploited. Namely after the first measurement of the counts $\bar{X}$ can only take integer values, after the second measurement of the counts (without doing a repump) $\bar{X}$ is multiple of $1/2$ and so on. The maximum amount of measurements without a repump is capped by the N_thr_red, which has value l. So l amount of libraries can be made (for each length of $\bar{X}$), where the l^{th} libraries have $(k+1) \cdot l$. Thirdly $\bar{X}$ is the Maximum Likelihood Estimator for the Poisson distribution, thus more observations should give a better estimation of the parameter λ. Discarding previous observations almost seems ignorant in a certain sense.

However there are some limitations to this implementation. For example the dt cannot be lowered from the value of 50 µs if no other measures are taken to increase N_tot, as then the normal approximation of the Poisson does not hold anymore. Such a measure could be to increase the intensity of the laser. Speeding up the simulation time to do more iterations would be a major objective for this implementation, to enable reliable conclusions trends from the data.

The Wilcoxon signed-rank test implementation appears to be a bit slower than the standard implementation wit regard to mean time till success. However it has also significantly lower spectral diffusion after passing the test, compared to the standard implementation. Although it has some practical drawbacks, namely it requires fast calculation of a computationally expensive test statistic, with good computing power this should not be a problem. More extensive research on this implementation could be done. Then the speeding up the simulation time to do more iterations would be a major objective for this implementation, to enable reliable conclusions trends from the data.

List of references

[1] N. Kalb, *Diamond-Based Quantum Networks with Multi-Qubit Nodes*, Ph.d. thesis, Delft University of Technology, 2018.

[2] G. Grimmett and D. Welsh, *Probability: An Introduction*, Oxford, Oxford University Press, 2017.

[3] M. Taboga, *Lectures on probability and statistics*, digital textbook, 2010.

Accessed on: 09-07-2020, via `https://www.statlect.com`

[4] S. Nadarajah, *A generalized normal distribution*, Journal of Applied Statistics, 32:7, 685-694, 2005.

[5] F. Bijma, M. Jonker and A. van der Vaart, *An Introduction to Mathematical Statistics*, Amsterdam, Amsterdam University Press, 2016.

[6] F. Wilcoxon, *Individual Comparisons by Ranking Methods*, Biometrics Bulletin, Vol. 1, No. 6., p. 80-83, 1945.

[7] F. Jelezko and J.Wrachtrup, *Single defects centres in diamond: A review*, Physica Status Solidi A, Vol. 203, p. 3207-3225, 2006.

[8] M. W. Doherty, N. B. Manson, P. Delaney and L. C. L. Hollenberg, *The negatively charged nitrogen-vacancy centre in diamond: The electronic solution*, New Journal of Physics 13, 025019, 2011.

[9] M. W. Doherty et al., *The nitrogen-vacancy colour centre in diamond*, Physics Reports 528, 1, 2013.

[10] D. Leibfried, R. Blatt, C. Monroe and D. Wineland, *Quantum dynamics of singletrapped ions*, Reviews of Modern Physics 75, 281, 2003.

[11] A. Lenef, S. C. Rand, *Electronic structure of the N-V center in diamond: Theory*, Physical Review B, Vol. 53, N. 20, 1996.

[12] S. Prawer, I. Aharonovich, *Quantum Information Processing with Diamond: Principles and Applications*, Elsevier, 2014.

[13] A. Browaeys et al., *Current Trends in Atomic Physics*, Oxford, Oxford University Press, 2019.

[14] Ph. Tamarat, T. Gaebel, J. R. Rabea, et al., *Stark Shift Control of Single Optical Centers in Diamond*, Phys. Rev. Lett. 97, 083002, 2006.

[15] R. P. Mildren, J. Rabeau, *Optical Engineering of Diamond*, Weinheim , Wiley-VCH Verlag GmbH and Co., 2013.

[16] L. Robledo, H. Bernien, I. van Weperen and R. Hanson, *Control and Coherence of the Optical Transition of Single Nitrogen Vacancy Centers in Diamond*, Physical Review Letters 105, 177403 ,2010.

[17] N. Aslam, G. Waldherr, P. Neumann, F. Jelezko and J. Wrachtrup, *Photo-induced ionization dynamics of the nitrogen vacancy defect in diamond investigated by single-shot charge state detection*, New Journal of Physics 15, 013064, 2013.

[18] H. Bernien, *Control, measurement and entanglement of remote quantum spin registers in diamond*, Ph.d. thesis, Delft University of Technology, 2014.

[19] Bernien, H., Hensen, B., Pfaff, W. et al., *Heralded entanglement between solid-state qubits separated by three metres*, Nature 497, 86–90, 2013.

[20] W. Pfaff, *Quantum Measurement and Entanglement of Remote Quantum Spin Registers in Diamond*, Ph.d. thesis, Delft University of Technology, 2013.

[21] W. Pfaff et al., *Unconditional quantum teleportation between distant solid-state quantum bits*, Science, Vol. 345, p. 532, 2014.

[22] B. Hensen, Quantum Nonlocality with Spins in Diamond, Ph.d. thesis, Delft University of Technology (2016).

[23] J. Bakermans, *Stable Emission and Excitation of the Nitrogen-Vacancy Centre for Quantum Communication*, Master's thesis, Leiden University (2016).

[24] *Numba: A high performance Python compiler*, `http://numba.pydata.org/`, Accessed on: 09-07-2020.

[25] G. Alves, Y.K. Yu. *Accuracy Evaluation of the Unified P-Value from Combining Correlated P-Values*, PLoS ONE 9(3): e91225, 2014.

[26] M. Veraar, *Real Analysis*, Lecture notes, Delft University of Technology, 2019.

[27] G. Grimmett and D. Stirzaker, *Probability and Random Processes*, Oxford, Oxford University Press, 2001.

[28] M. Winkel, *Part B Applied Probability*, Lecture notes, Oxford, 2007. Accessed on: 09-07-2020, via `http://www.stats.ox.ac.uk/~winkel/bs3a07l9-10.pdf`

Appendices

Appendix A: Law of Large Numbers

Since we are dealing with stochastic processes, we need to have some certainty that the values we will obtain by averaging over a large amount of iterations really represent the needed parameters. This can be shown by the Law of Large Numbers (LLN), which exists in two forms the strong law and the weak law. This strong and weak refers to the type of convergence.

In this section first Markov's and Chebyshev's inequalities will be proven. Thereafter the Weak Law of Large Numbers is proven under the condition that the variance is finite. Next the Borel-Cantelli lemma is proven, followed by a lemma that is also used for the proof of the Strong Law of Large Numbers. Then the proof of the Strong Law of Large Numbers of large numbers is given under the condition that the fourth moment is finite.

These theorems will not be used directly in this report, but they are the reason why these simulations are meaningful.

Markov's and Chebyshev's inequalities

First Markov's and Chebyshev's inequalities are proves to provide a bound on the probability. This is then used in teh proofs of the Law of Large Numbers.

Theorem 1. ***(Markov's inequality)*** *Let X be any non-negative random variable, then for $t > 0$:*

$$\mathbb{P}(X \geq t) \leq \frac{\mathbb{E}(X)}{t}$$

Proof. We will prove it for the case that X has a continuous probability density function $f_X(x)$. In case the probabilities are discrete, it can be proved analogously or one could consider to transformed the discrete pmf into a continuous pdf using delta peaks.

Let $t > 0$ be given and X be a non-negative random variable, then:

$$\mathbb{E}(X) = \int_{-\infty}^{\infty} x f_X(x)dx = \int_{0}^{\infty} x f_X(x)dx = \int_{0}^{t} x f_X(x)dx + \int_{t}^{\infty} x f_X(x)dx \leq$$

$$\int_{t}^{\infty} x f_X(x)dx \leq \int_{t}^{\infty} t f_X(x)dx = t \int_{t}^{\infty} f_X(x) = t\,\mathbb{P}(X \geq t),$$

where we use the fact that X is non-negative and that thus the expectation operator is monotonically increasing function. Thus we obtain $\mathbb{E}(X) \geq t\,\mathbb{P}(X \geq t)$, rewriting this gives:

$$\mathbb{P}(X \geq t) \leq \frac{\mathbb{E}(X)}{t}.$$

□

Theorem 2. ***(Chebyshev's inequality)*** *If X is a random variable with finite variance, then $\forall t > 0$:*

$$\mathbb{P}(|X - \mathbb{E}(X)| \geq t) \leq \frac{Var(X)}{t^2}$$

.

Proof. Define $Y = (X - \mathbb{E}(X))^2$. Then we can use Markov's inequality (1), this gives:

$$\mathbb{P}(|X - \mathbb{E}(X)| \geq t) = \mathbb{P}((X - \mathbb{E}(X))^2 \geq t^2) = \mathbb{P}(Y \geq t^2) \leq \frac{\mathbb{E}(Y)}{t^2} = \frac{Var(X)}{t^2},$$

where we have used the definition of the variance. □

Weak Law of Large Numbers

The idea for this proof stems from [3].

Theorem 3. ***(Weak Law of Large Numbers (WLLN))*** *Let $(X_n)_n$ with $n \in \mathbb{N}$ be a sequence of random variables such that:*

1. *X_n are mutually independent*
2. *$\forall n$, $\mathbb{E}(X_n) = \mu$*
3. *$\forall n$, $Var(X_n) = \sigma^2$*

Then

$$\frac{1}{N}\sum_{i=1}^{N} X_i \to \mu \text{ in probability as } N \to \infty.$$

Proof. To prove: $\forall \epsilon > 0$, we have $\mathbb{P}(|\frac{1}{N}\sum_{i=1}^{N}(X_i - \mu)| \geq \epsilon) \to 0$ as $N \to \infty$. Take $\epsilon > 0$ arbitrary. Then:

$$\mathbb{P}(|\frac{1}{N}\sum_{i=1}^{N}(X_i - \mu)| \geq \epsilon) \leq \frac{1}{\epsilon^2} Var(\frac{1}{N}\sum_{i=1}^{N} X_i) = \frac{1}{N^2\epsilon^2}\sum_{i=1}^{N} Var(X_i) = \frac{1}{N^2\epsilon^2} N\sigma^2 = \frac{\sigma}{N\epsilon^2},$$

where we used Chebyshev's inequality (2) and the properties of the variance operator for independent variables. So now we take the limit:

$$0 \leq \lim_{N\to\infty} \mathbb{P}(|\frac{1}{N}\sum_{i=1}^{N}(X_i - \mu)| \geq \epsilon) \leq \lim_{N\to\infty} \frac{\sigma}{N\epsilon^2} = 0$$

So we obtain:

$$\frac{1}{N}\sum_{i=1}^{N}(X_i - \mu) \to 0 \text{ in probability as } N \to \infty.$$

□

Strong Law of Large Numbers

Ideas for the proof of the Borel-Cantelli lemma stem from [26] and [27].

Lemma 1. ***(Borel-Cantelli Lemma)*** *Let $A = \bigcap_{n\geq 1}\bigcup_{m\geq n} A_m$ be the event that infinitely many of the events A_n occur. Then:*

$$\sum_{n\geq 1} \mathbb{P}(A_n) < \infty \quad \Rightarrow \quad \mathbb{P}(A) = 0$$

Proof. Note that $\forall n \geq 1$ we have that $A \subseteq \bigcup_{m\geq n} A_m$. Thus:

$$0 \leq \mathbb{P}(A) \leq \mathbb{P}(\bigcup_{m\geq n} A_m) \leq \sum_{m\geq n} \mathbb{P}(A_m) \to 0$$

for $n \to \infty$, as we have that $\sum_{n\geq 1} \mathbb{P}(A_n) < \infty$ and this means that $\mathbb{P}(A_n) \to 0$ sufficiently fast as $n \to \infty$. □

The proof of the following lemma and the Strong Law of Large Numbers was heavily inspired by [27] and [28].

Lemma 2. *Let $(X_n)_n$ with $n \in \mathbb{N}$ be a sequence of independent and identically distributed (i.i.d) random variables with $\mathbb{E}(X_1^4) = R < \infty$ and $\mathbb{E}(X_1) = \mu$. If we define $S_n := \sum_{i=1}^{n} X_i$, then there exists a constant $K < \infty$ such that $\forall n \geq 1$:*

$$\mathbb{E}\left((S_n - n\mu)^4\right) \leq Kn^2.$$

Proof. Note that $0 \leq Var(X_1^2) = \mathbb{E}(X_1^4) - (\mathbb{E}(X_1^2))^2$, thus that $(\mathbb{E}(X_1^2))^2 \leq R$. Define $Y_k := X_k - \mu$, then we have $Z_n := \sum_{i=1}^{n} Y_i = S_n - n\mu$. Thus:

$$\mathbb{E}\left(T_n^4\right) = \mathbb{E}\left(\sum_{i=1}^{n} Y_i^4\right) = n\mathbb{E}(Y_1^4) + \begin{pmatrix} 4 \\ 2 \end{pmatrix}\begin{pmatrix} n \\ 2 \end{pmatrix}\mathbb{E}(Y_1^2 Y_2^2) = n\mathbb{E}(Y_1^4) + 3n(n-1)\left(\mathbb{E}(Y_1^2 Y_2^2)\right)\right) \leq Kn^2,$$

where we have chosen $K = 4\max\left(\mathbb{E}(Y_1^4), \mathbb{E}(Y_1^2 Y_2^2)\right)$ which is a finite number by the fact that $\mathbb{E}(X_1^4) = R < \infty$. Both $\begin{pmatrix} 4 \\ 2 \end{pmatrix}\begin{pmatrix} n \\ 2 \end{pmatrix}$ and $n = \begin{pmatrix} n \\ 1 \end{pmatrix}$ come from the amount of combinations in which we can make these terms. In this calculation we have used the fact that the Y_i are independent, thus $\forall i, j, k, l$ with $i \neq j \neq k \neq l$ we have $\mathbb{E}(Y_i^3 Y_j) = 0$, $\mathbb{E}(Y_i^2 Y_j Y_k) = 0$ and $\mathbb{E}(Y_i Y_j Y_k Y_l) = 0$.

□

Theorem 4. ***(Strong Law of Large numbers (SLLN))*** *Let $(X_n)_n$ with $n \in \mathbb{N}$ be a sequence of independent and identically distributed (i.i.d) random variables with $\mathbb{E}(X_1^4) = R < \infty$ and $\mathbb{E}(X_1) = \mu$. Then:*

$$\frac{S_n}{n} := \frac{1}{n}\sum_{i=1}^{n} X_i \to \mu \text{ almost surely.}$$

Proof. First note that $\mathbb{E}\left(\left(\frac{S_n}{n} - \mu\right)^4\right) = \mathbb{E}\left(\left(\frac{1}{n}(S_n - n\mu)\right)^4\right) = \frac{1}{n^4}\mathbb{E}\left((S_n - n\mu)^4\right) = Kn^{-2}$ by lemma (2) and the linearity of the expectation operator. Now we can apply Markov's inequality (1) to the following:

$$\mathbb{P}\left(\frac{1}{n}\left|S_n - n\mu\right| \geq n^{-\gamma}\right) = \mathbb{P}\left(\left(\frac{S_n}{n} - \mu\right)^4 \geq n^{-4\gamma}\right) \leq \frac{\mathbb{E}\left((S_n/n - \mu)^4\right)}{n^{-4\gamma}} = Kn^{-2+4\gamma}$$

Now we define for $\gamma \in (0, \frac{1}{4})$ the following: $A_n = \left\{\frac{1}{n}\left|S_n - n\mu\right| \geq n^{-\gamma}\right\}$

Note that we have $\sum_{n\geq 1}\mathbb{P}(A_n)$ is finite, since for $\gamma \in (0, \frac{1}{4})$ we have $\sum_{n=1}^{\infty} Kn^{-2+4\gamma}$ is a convergent series (it is a p-series multiplied by a constant). Thus we may use the Borel-Cantelli lemma (1). So we conclude $\mathbb{P}(A) = 0$, where $A = \bigcap_{n\geq 1}\bigcup_{m\geq n} A_n$. Thus we have that $\mathbb{P}(A^c) = 1$ and the event A^c occurs if and only if $\exists N$ such that $\forall n \geq N$ we have that $\left|\frac{S_n}{n} - \mu\right| < n^{-\gamma}$. So there exist only finitely many instances (namely $n \leq N$) where $\left|\frac{S_n}{n} - \mu\right| \geq n^{-\gamma}$. By definition this means:

$$\frac{S_n}{n} \to \mu \text{ almost surely.}$$

□

Appendix B: Normal approximation

For large values of λ, the Poisson distribution may be approximated by the Normal distribution with mean λ and variance λ. It will be proven using the fact that convergence of moment generating function (mgf) implies convergence in distribution. We will however not elaborate on this last fact, it can be found in [3] under Theorem 8.27 (Continuity theorem). But first we will prove the following lemma.

Lemma 3. *Let X have moment generating function $M_X(t)$ and $\forall a, b \in \mathbb{R}$ we define $Y = aX + b$, then we have that $M_Y(t) = e^{bt} M_X(at)$*

Proof. By using the definition of the mgf and linearity of the expectation operator we obtain:

$$M_Y(t) = M_{aX+b}(t) = \mathbb{E}[e^{(aX+b)t}] = \mathbb{E}[e^{atX+bt}] = \mathbb{E}[e^{atX} e^{bt}] = e^{bt}\mathbb{E}[e^{(at)X}] = e^{bt} M_X(at).$$

Thereby proving the result. □

Now that we can use the lemma, we will prove the Normal approximation to the Poisson distribution.

Theorem 5. *Let X be Poisson distributed with parameter λ. Let $\lambda \to \infty$, then $X \to N(\lambda, \lambda)$. In other words if we define $Y = \frac{X-\lambda}{\sqrt{\lambda}}$ which is the standardized form, then $Y \to N(0, 1)$ in distribution.*

Proof. Remark that two notations will be used for the exponential function, namely $\exp(x)$ and e^x. We will show that the moment generating function for Y tends to the moment generating function of a Normal distribution. Recall that the MGF of a standard Normal distribution is $M_N(t) = \exp\left(\frac{1}{2}t^2\right)$ and that the MGF of a Poisson distribution with parameter λ (in our case X) is $M_X(t) = \exp(\lambda(e^t - 1))$. So to show: $M_Y(t) \to M_N(t)$ as $\lambda \to \infty$. Note that $Y = \frac{1}{\sqrt{\lambda}}X - \sqrt{\lambda}$, so we may apply the lemma. $M_Y(t) = \mathbb{E}[e^{Yt}] = e^{-\sqrt{\lambda}t} M_X(\frac{t}{\sqrt{\lambda}})$. Thus:

$$M_X(\frac{t}{\sqrt{\lambda}}) = \exp\Big(\lambda(e^{\frac{t}{\sqrt{\lambda}}} - 1)\Big) = \exp\left(\lambda(1 + \frac{t}{\sqrt{\lambda}} + \frac{t^2}{2\lambda} + \frac{t^3}{3!\lambda^{\frac{3}{2}}} + \cdots - 1)\right) =$$

$$\exp\left(t\sqrt{\lambda} + \frac{t^2}{2} + \frac{t^3}{3!\sqrt{\lambda}} + \dots\right),$$

where we have used the definition of the exponent. So then we get that:

$$M_Y(t) = e^{-\sqrt{\lambda}t} \exp\left(t\sqrt{\lambda} + \frac{t^2}{2} + \frac{t^3}{3!\sqrt{\lambda}} + \dots\right) = \exp\left(\frac{t^2}{2} + \frac{t^3}{3!\sqrt{\lambda}} + \dots\right).$$

So as $\lambda \to \infty$,

$$M_Y(t) \to \exp\left(\frac{1}{2}t^2\right) = M_N(t)$$

□

In practice the approximation is already acceptable for $\lambda \approx 20$.

Appendix C: Emission spectrum

The emission spectrum of the NV center for both charge states is shown.

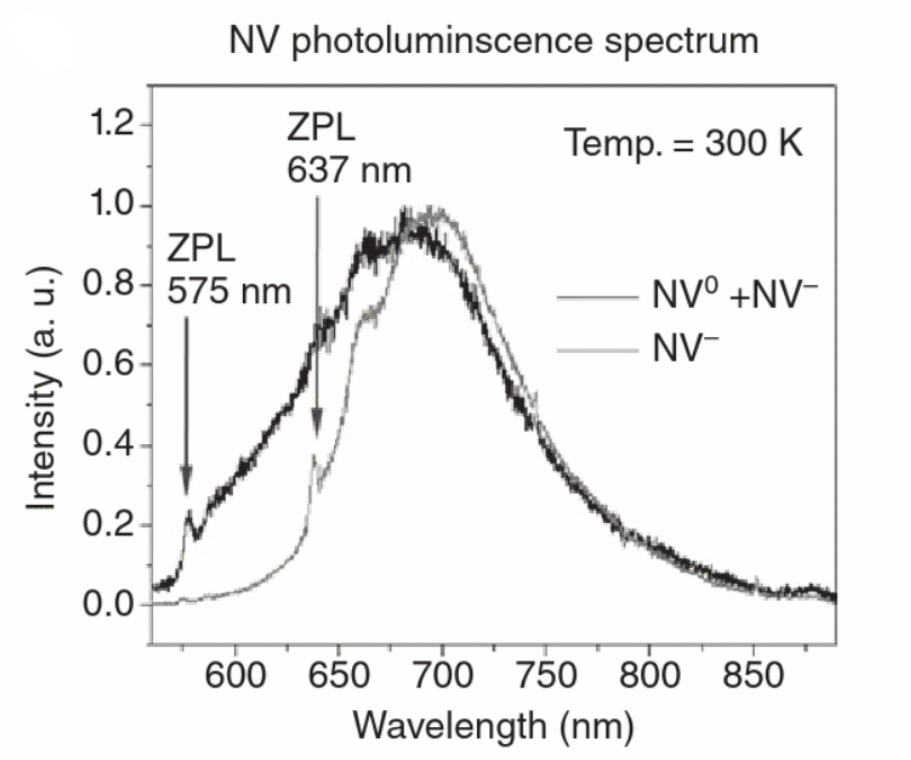

Figure 30: The figure shows the emission spectra of both NV^- and NV^0. Immediately the difference in wavelength of the respective zero-phonon lines can be seen. The figure is taken from: [17].

Appendix D: Code optimization

For further optimization of the code the Python library Numba [24] is used. Numba provides several methods to optimize code, allowing for a faster running time.

JIT Compilation to C

One of the main problems with simulating in Python is that it runs very slowly compared to other programming languages. To circumvent this we utilize Numba's JIT compilation in nopython mode [24]. This means our code is no longer run in the Python kernel, but is rather compiled to C bytecode. JIT, short for just-in-time compilation, is a method of execution where compilation occurs at run time as opposed to a priori. It furthermore allows for easier parallelization of the code, which will be discussed later. The downside is that only a limited number of functions are available.

By properly compiling the python code using Numba's JIT in nopython mode, we can ensure that the code runs close to optimally whilst still benefiting from the accessibility of Python.

Parallelization

Since we run the same procedure on each iteration, parallelization could pose a significant advantage to our running time. We can avoid that the cores need information from the previous iteration, which is running on another core, by looping over the whole process. Thus each core will pass this information on to itself. For example the resonance frequency after passing a CR-Check and being modified by a measurement is passed on this way.

In the case of our simulation the code is run on the CPU. The simulation is run on a Intel Core i7-7700HQ Processor with 8 logical cores, allowing us to run through the simulation with 8 NV centers, with the same input parameters with exception to the resonance frequency, simultaneously. It can even be regarded as one NV center as the effect of the 8 runs is averaged out over many iterations.

The benefit of parallelizing the code is almost an 8x increase of speed. On GPU computation platforms like CUDA, the effect of parallelization is way more significant, since this architecture is designed to perform calculations in parallel. This can be investigated in further research.

Appendix E: Results

Some figures belonging to the chapter of the results are shown here, to keep the chapter to a reasonable size.

Sigma variation 0-500 MHz

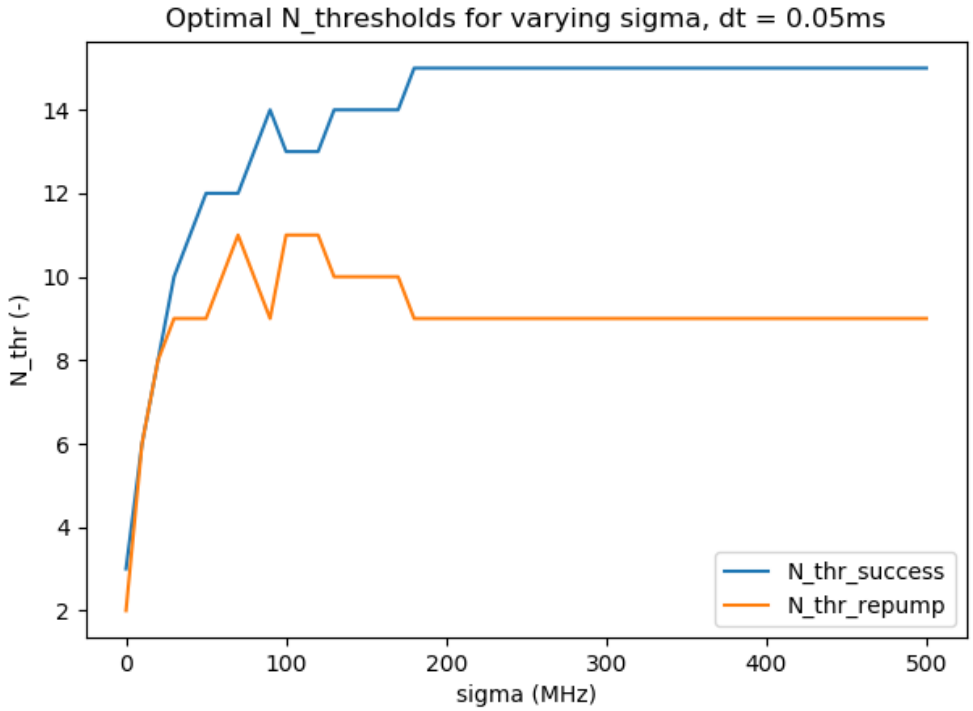

(a) Plot of the optimal values for threshold for success and the thresholds for repump over varying spectral diffusion.

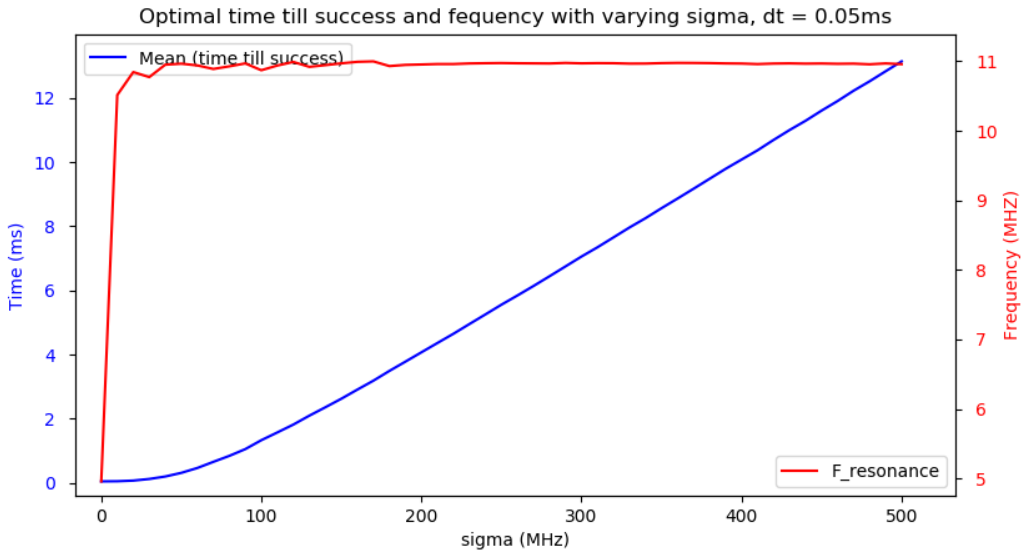

(b) Graph of the average resonance frequency on success and the mean time till success with varying sigma.

Figure 31: The results of a sigma variation from 0 to 500 MHz with dt = 50 µs.

2D Variation of sigma and dt

We can consider the 1D sweep of sigma and 1D sweep of dt just as strips of a larger picture. Thus we will perform a 2D variation of both sigma and dt at the same time. In this manner we hope to to uncover trends which are dependent on both parameters. The 2D sweeps show the computation power of our implementation. First we will take a look at the thresholds:

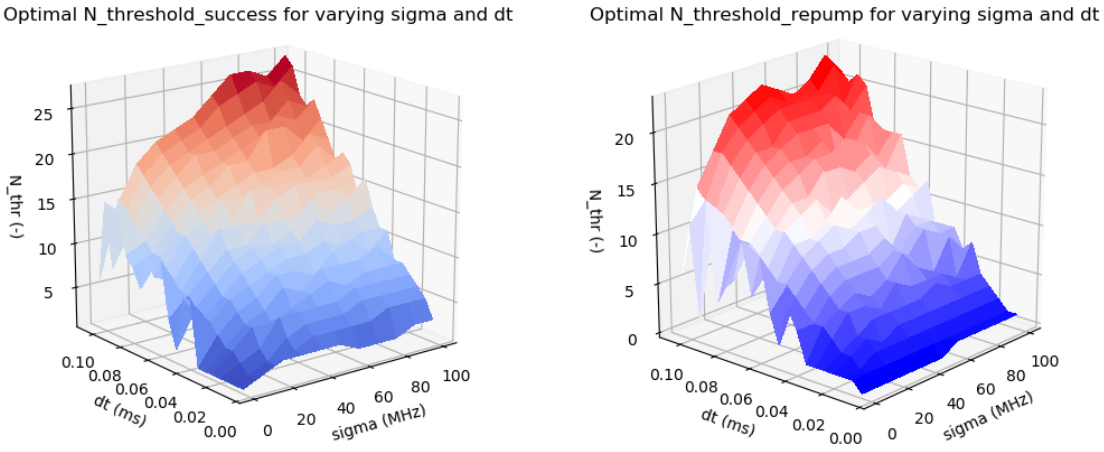

Figure 32: Plots of the optimal values of N_thr_success and N_thr_repump with varying spectral diffusion and laser duration.

Roughly the same pattern for both N_thr_success and N_thr_repump can be observed in Fig.32, only the repump threshold is a bit lower than the threshold for success. This seems also to be in accordance with the idea of threshold pairs.

Next we will look at the the mean time till success.

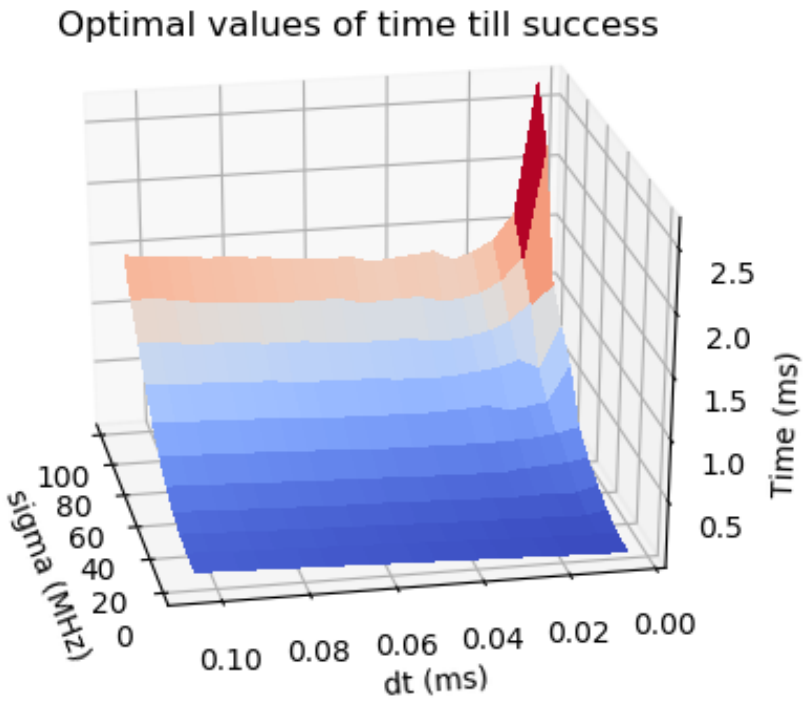

Figure 33: Plot of the average the mean time till success for the optimal values with varying spectral diffusion.

Again a minimum for sigma = 100 MHz is observed at 0.025 ms, which was previously also obtained in Fig.24b. Additionally it can be seen in Fig33 that for sigma = 0 MHz, dt = 0.005 ms is the optimal value. This gives an indication that this minimum moves along the dt axes, depending on the spectral diffusion of the defect. This effect can even to some degree be observed in the figure.

Now we will also look at the detected photon counts on success.

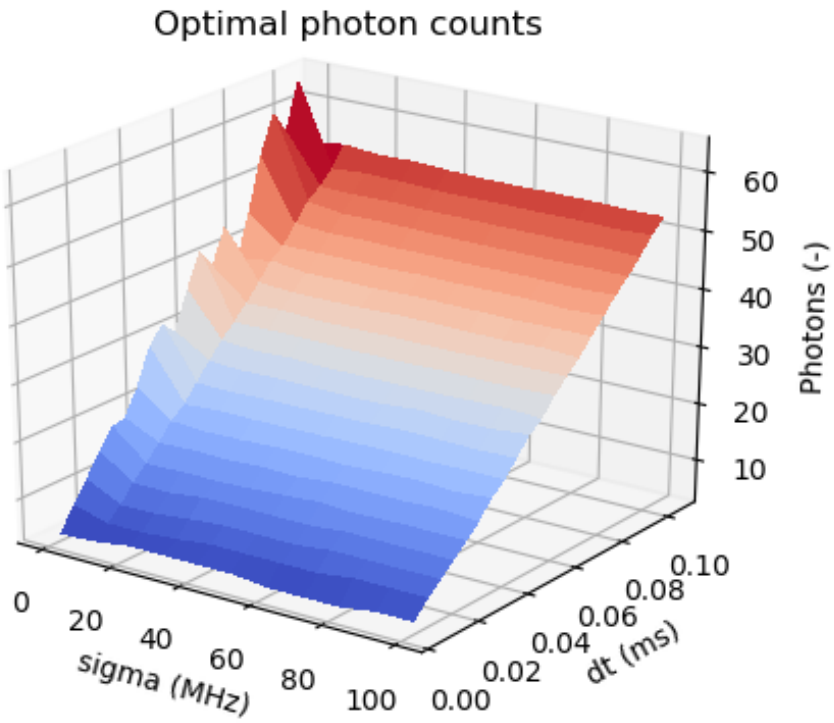

Figure 34: Plot of the average photon counts on success for the optimal values with varying spectral diffusion and laser length.

For 0 spectral diffusion the highest average photon counts, as then NV center is on resonance. From Fig.34 we can indeed see that the average photon counts after passing a CR-Check only depends on the length of the laser duration and not on the spectral diffusion of the defect. This is an indication that the NV center is always brought sufficiently on resonance by the CR-Check routine.

Appendix F: The code

All the code that was used in this project to run the simulations, acquire and process the data is available online via the following URL: `https://gitlab.com/uognjanovic/bep`.